COMPARISON OF RAINFALL ENERGY AND SOIL EROSION PARAMETERS FROM A RAINFALL SIMULATOR AND NATURAL RAIN

A Thesis presented to the Faculty of the Graduate School
University of Missouri-Columbia

In Partial Fulfillment
Of the Requirements for the Degree
Master of Science

---

by

WILLIAM T. GILMORE

Dr. Neil I. Fox and Dr. Allen L. Thompson,
Thesis Supervisors

MAY 2007

The undersigned, appointed by the Dean of the Graduate School, have examined the thesis entitled

COMPARISON OF RAINFALL ENERGY AND SOIL EROSION PARAMETERS

FROM A RAINFALL SIMULATOR AND NATURAL RAIN

Presented by William T. Gilmore

A candidate for the degree of Master of Science

And hereby certify that in their opinion it is worthy of acceptance.

Dr. Neil I. Fox

Dr. Allen L. Thompson

Dr. Anthony R. Lupo

Dr. Randall J. Miles

ACKNOWLEDGEMENTS

First and foremost, I would like to thank the University of Missouri-Columbia Department of Soil, Environmental, and Atmospheric Science. Many thanks go to my advisors, Dr. Neil Fox and Dr. Allen Thompson, for allowing me the opportunity to continue my education by earning a master degree in Soil, Environmental, and Atmospheric science. Your advice on research methods and ideas for the study are what made this possible. Also, thanks goes to Dr. Patrick Market and Dr. Anthony Lupo for teaching me the ways of Atmospheric Science through my undergraduate and graduate years. Your advice on career opportunities and additional research experience with Research on Convective Snows (ROCS) and leadership skills gathered over the years is greatly appreciated. Without the encouragement of all four professors mentioned here would I have made it this far. Thanks also goes to Sharon Burnham for providing the opportunity to get to know the department through my work study experience, and providing any assistance she could provide whenever requested. Without Sharon, the Atmospheric Science Department "mother figure", myself and the many people whose lives she has made at least a little bit simpler, would probably have not accomplished what we have today.

Thanks and credit also goes to the organization that funded this research. Thanks go to the Missouri Water Resource Research Center for the ability to allow research to be conducted on the topic of rainfall kinetic energy and impact on soil erosion.

The many people involved with the research project deserve special thanks since much of this project would not have been possible with out their assistance and advice. First, the data used in this study would not have existed if it were not for the University of North Dakota's School of Aerospace Engineering, Atmospheric Science branch loaning the raindrop imaging system. Dr. Paul Kucera and Graduate student Andrew Newman deserve special thanks for the training and troubleshooting advice on the imaging system. Acknowledgment also goes to Cliff Mongler, from the Agriculture Engineering shop, for designing soil trays used in the soil erosion aspect of this study. Other persons involved include Steven Lack for preparing the rain gauges and anemometers, and George Limpert for assistance with troubleshooting the analysis software with MATLab. Aaron Naeger, Nathan Davis, Chris Foltz, and Cody Fritz are all thanked for their time and effort in assisting in certain aspects of this study, from the late nights at South Farm gathering data, or setting up equipment in the Hydrology Laboratory. Without all those mentioned here, my research would not have been completed.

The Undergraduate and Graduate students throughout my time here at Mizzou had an irreplaceable impact on my life. The many activities I was involved with the Meteorology Club and the Mizzou Storm Chase team allowed me to meet the most interesting people in my life. Whether camping and barbequing with Larry Smith, Christina Crowe, Kristen Mihalka, Ali Kolieny (just to mention a few), or seeing the incredible displays of Mother Nature while storm chasing with Dan Hinch, Jeff La Montia, Chris Melick, or Caleb Witt-Schulte, your antics and comedy over the years will never be forgotten. My roommates over the past two years, Dave Jankowski, Amy Becker, and Brian Pettegrew, deserve credit for putting up with my craziness day in and day out. Also, thanks goes to those in my Weather Briefing class I instructed in the WS2006. Without the opportunity for me to spread my knowledge to those students, and by learning more myself from their ideas and questions, will I have had the confidence of knowing what I am capable of accomplishing. To all of those that have supported and encouraged me throughout my college career here at Mizzou, I thank you.

Those closest to me deserve the greatest acknowledgment. If it were not for Chris Schultz's sarcasm, excitement, motivation, and friendship over the years, I would have not believed in my potential, not just in my academics, but in life in general. He has exposed me to

many new things, people, and places that I will remember forever. Cody Fritz, Marc Dahmer, and Emily (Rosie) Sutton hold a special place in my heart. Their constant encouragement and support has pushed me further and further, continually convincing me not to give up, and have helping me get over the modest view I have of myself. They all have had one of the greatest influences of anyone throughout my life. Without Rosie's smiling face, creativity, and love of life, I would have not believed that things really do happen for a reason. Through the struggles, the excitement, and the highs and lows, those four people have always been there to cheer me on, and given me the strength to continue. I thank you, and love you all dearly.

Finally, if it were not for my family back home, none of my experiences here at Mizzou and my entire college career would have existed. They were the ones that first pushed me to get out and experience life when the opportunity presented itself. They convinced me that if I did not do something now, I may never get the chance to do it again. The love, laughter, encouragement, and discipline they have instilled in me have made me the person I am today, and my accomplishments, past and future, will result in some part because of them. There is not enough thanks and gratitude that could ever be expressed for their love and support, and I know that with anything I

ever do, they will be there to support me. For this, I love and thank you very much.

For those that have not been mentioned here, do not worry. Your influence in this work will never be forgotten. I thank you all very much!

TABLE OF CONTENTS

LIST OF FIGURES

Figure **Page**

LIST OF TABLES

ABSTRACT

Numerous studies have used artificial rainfall to quantify relationships for runoff and soil detachment. Application of these results to natural rainfall conditions is dependent in part on how well artificial rainfall mimics these natural conditions. According to recent research, the increased velocity of droplets due to wind can account for up to one quarter of the total kinetic energy of the raindrops (Helming 2001). However, the results presented here show that about one-half of the total kinetic energy was estimated from horizontal wind. This thesis discusses the differences in kinetic energy estimated from horizontal compared to Helming (2001). Also, turbulence, while difficult to quantify, can enhance the error in gathering soil loss data from the field in convective rainfall situations due to splash out.

In this study, a rainfall imaging system, including a digital camera to capture images of raindrops, has been used to determine the drop-size distributions of natural rain in Missouri. These observations have been compared to those from an indoor gravity rainfall simulator. This thesis reports the results of the drop-size distribution (DSD) intercomparison, where a gamma distribution curve was expected, but a special form of a gamma distribution (exponential distribution) was found.

While there are differences between the shapes of the DSDs, the most significant difference between the natural and simulated rain observed in the cases to date is the temporal variation of the natural rain. The fluctuations in rainfall rate prevent the consistent surface pooling of water that occurs in most simulated events.

Chapter 1

Introduction

Soil loss is a major issue among the agriculture industry and water management fields across the entire globe (Eswaran *et al*. 2001). Whether it is soil loss conservation, water quality control, or preparation for extreme weather phenomena, predicting soil loss caused by rainfall can be performed numerically by engineers. They can then design appropriate erosion or soil displacement prevention techniques. Many models used to predict soil erosion are based on data gathered in the 1940s, such as the Universal Soil Loss Equation (USLE), and the revised USLE or RUSLE (Renard *et al*. 1997). These models are based on assumed rainfall characteristics from studies that used flour pellet or blotting paper methods to determine drop size distribution (DSD) (Laws and Parsons 1943; Marshall and Palmer 1948) useful in determining rainfall kinetic energy. Technology today allows for the use of optical disdrometers to gather more detailed and site-specific raindrop size distributions determined from larger samples. The data collection time can cover the entire storm duration or rain event, which allows one to fully capture the temporal variations in rain DSDs. Capturing the variations also minimizes human error

involved in data collection compared to previous methods.

Another aspect of DSDs deals with radar rainfall intensity and accumulation estimates. Radar reflectivities are based on the diameters of the particles scattering radiation back to the radar receiver. Large variations in radar reflectivity occur with relatively small changes in diameter of particles, since the reflectivities are related to the diameters of objects raised to the sixth power. Therefore, variations in DSDs associated with particles in the atmosphere, specifically hydrometeors in this case, can have a great impact on the derived algorithms used in rainfall rate estimation, rainfall kinetic energy, and storm intensities associated with radar. Any benefits yielded from fine-tuning the DSD-Radar reflectivity relationship will benefit operational meteorologists by helping forecasters identify areas that are under the greatest threat of prolonged and threatening heavy rainfall totals. This will allow forecasters the ability to use more accurate remote sensing tools when critical decisions are required for issuing warnings for flash flooding, the number one cause of severe weather fatalities in the United States. The goal of this thesis will focus on the relationship of DSDs to soil loss and relating simulated rainfall to natural events.

1.1 Statement of Thesis

The purpose of this study is to examine models of rainfall DSD and their application in models of soil erosion.

The detachment of soil that is lost to sheet and rill erosion during rainfall events is a function of the kinetic energy of the rain that impacts the soil. As rain consists of a spectrum of drop sizes, the kinetic energy is dependent upon the nature of the distribution of those sizes. In particular, larger drops have both greater mass and vertical terminal velocity such that a disproportionate amount of energy and potential erosion results from the action of a small number of large drops.

Recently, studies of rainfall using meteorological radars have revealed that the traditional parameterization of the DSD may be inaccurate and that natural DSDs can take different forms (e.g. Ulbrich and Atlas 1998; Illingworth 2003). Laboratory studies of rainfall generated soil erosion have been conducted using rainfall simulators. However, these indoor simulators are limited to reproducing raindrop vertical velocities, whereas the kinetic energy of the drops in natural rain is a product of both the drop's vertical (terminal) velocity and its horizontal (wind generated) velocity. Laboratory studies are unable to replicate the total momentum of the drops as they cannot produce the lateral motion which can be comparable to, or greater than, the

vertical velocity (Lack and Fox 2003). The angle of incidence of the rain striking the surface is also important in the erosion process. In addition, the DSD produced in laboratory studies often displays considerable differences compared with natural rainfall because of the difficulty in getting adequate drop numbers in the very small and very large sizes (Thompson and Ghidey 2000).

This research will attempt to resolve the differences between the assumed DSD and total kinetic energy used for most soil erosion calculations by comparing the DSD of 'rain' generated in the laboratory for soil erosion studies with observations of natural rainfall in the field. The error can then be assessed in the conversion of laboratory studies of soil erosion to actual soil loss. This could lead to better estimates of natural soil loss over wide areas and a better understanding of soil transport into waterways. The objectives of this study are to:

- Examine the raindrop size spectra for natural rain as a function of different rainfall intensities, and the ability to reproduce this in laboratory studies.
- Compare the detailed drop-size spectra measurements of natural rain to standard measurements of rainfall intensity observed using rain gauges.

- Compare the timing of water ponding and amount of soil loss generated by natural and simulated rainfall.

With the purpose and objectives stated for this study, specific hypotheses will be tested. Those hypotheses are:

- Simulated rainfall has the same characteristics as natural rainfall for drop kinetic energy as a function of rainfall intensity.
- Natural rainfall DSD is best represented by a gamma curve with a shape factor (μ) that equals zero (exponential curve).
- Estimation of kinetic energy contributions from horizontal wind influence account for a significant portion of the total kinetic energy contained within some rainstorms.
- Simulated rainfall produces the same soil loss, ponding, and runoff as natural rainfall for events of equal rainfall intensity.

Chapter 2

Literature Review

The management practices of soil and soil loss conservation have been a significant topic of research for the agriculture industry and water management field world wide. The models predicting soil erosion, such as the Universal Soil Loss Equation (USLE), and the revised USLE or RUSLE (Renard *et al*. 1997), are based on data gathered in the 1940s. The RUSLE uses 30-minute average rainfall intensity in calculating the kinetic energy, then relating that kinetic energy to the observed soil loss from large soil plots. The kinetic energy-rainfall rate relationship is calculated from assumed DSD data that used flour pellet or blotting paper methods to determine DSD from Laws and Parsons 1943 and Marshall and Palmer 1948 (henceforth LP/MP). The proposed drop size distribution (DSD) found by Marshall and Palmer (1948) is generally accepted as a reasonable representation of natural rainfall in low intensity, non-convective storms in the mid-latitudes (rainfall rates of 1 to 23 mm h^{-1} in this study). However, this method may not correctly represent the DSD produced by convective or short term, high intensity storms common in portions of the central United States.

Knowing natural raindrop distributions during rain events can improve soil erosion prediction by developing or adjusting current soil loss prevention techniques.

Mason and Andrews (1960) found median volume drop diameters to increase when going from rainfall associated with warm fronts, such as moderate showers, to mature thunderstorms. A study at Island Beach, NJ was also able to separate drop size distributions during storms associated with pre-cold front convection and cold-type occlusions (Van Dijk *et al*. 2002). In general, at a particular rainfall intensity, kinetic energy also increased from moderate rain to mature thunderstorm rainfall. Van Dijk *et al*. (2002) also presented a study that suggested that rainfall DSD (specifically median drop size diameter) was positively related to air temperature. However, this temperature effect likely reflects differences in storm type, rather than air temperature alone. For example, it is likely that rainfall in summer may have fallen as convective thunderstorms which are generally associated with larger drop sizes. No specific synoptic conditions were given in this study. Overall, it appears that the median raindrop size at a particular rainfall intensity decreases with increasing latitude and increases when going from warm frontal rain and drizzle to more energetic rainfall associated with cold fronts and thunderstorms.

2.1 Exponential Distributions

Originally it was believed that DSDs followed an exponential distribution based on results from flour pellet studies from LP/MP. This type of DSD was generally accepted for low-intensity, non-convective rainfall, or those rainstorms where soil loss from raindrop kinetic energy is low. The exponential DSD described by Marshall and Palmer (1948) is shown by

$$N(D) = N_T \exp(-\Lambda D) \tag{2.1}$$

where N(D) is the concentration (m^{-3}) of drops of diameter D (mm), N_T is the total number of drops, and Λ is a parameter related to the median drop diameter of the size spectrum (mm^{-1}):

$$\Lambda = \frac{3.67}{D_0} \tag{2.2}$$

where D_0 is the median drop size diameter. This denotes the drop size for which half the total volume of water of the drops is smaller, and half is contained in drops larger than this diameter. Figure 2.1 shows an example of what DSDs would mimic using this parameterization.

2.2 Gamma Distributions

Natural raindrop distributions are now known to be better represented by a statistical gamma distribution for those convective, high energy rainstorms (e.g. Testud *et al*. 2001). A brief description of

the gamma distribution method (example shown in figure 2.2) is shown using the following expression:

$$N(D) = N_T D^{\mu} \exp(-\Lambda D) \tag{2.3}$$

The value of μ is the order of the gamma distribution, which can range from 0 to 10, typically toward the lower end of the range. In this case, Λ is represented by

$$\Lambda = \frac{(3.67 + \mu)}{D_0} \tag{2.4}$$

to account for the independent values of μ.

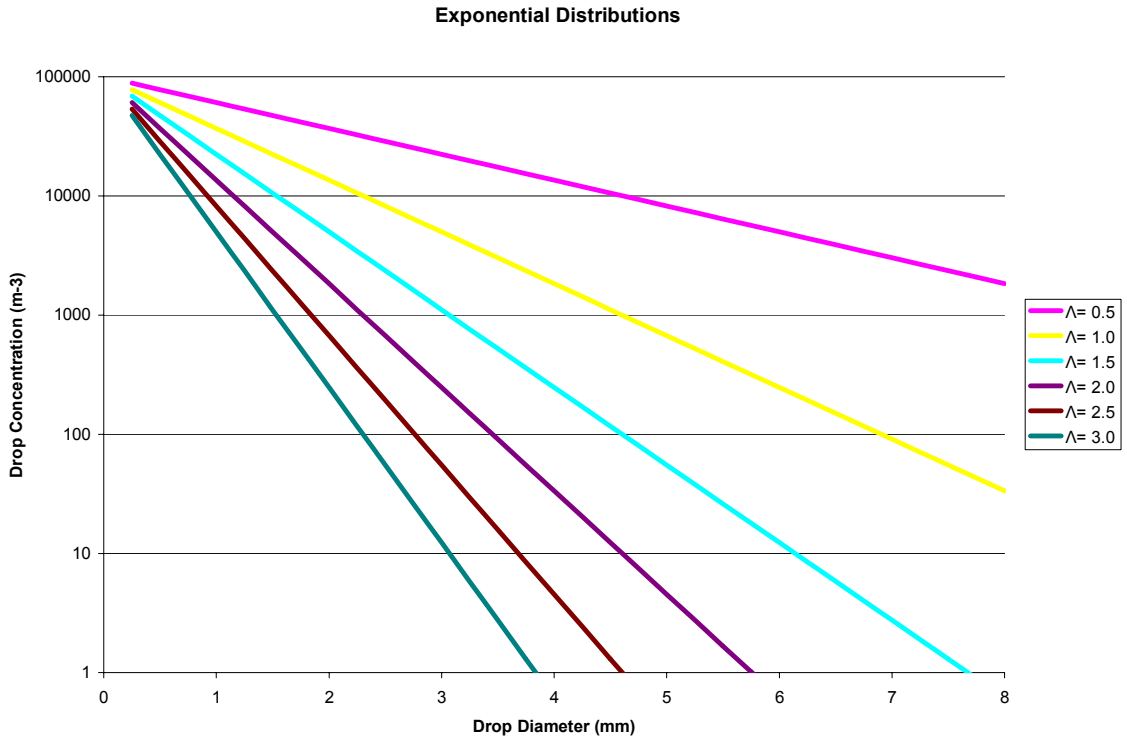

Figure 2.1 : Example of exponential DSDs, with different values of Λ, changing D_0.

As the value of μ is increased, the concentration of the larger drops is reduced, while the median drop size increases. This will lead to a narrower DSD, reducing the total kinetic energy flux of the falling drops. This allows μ to be considered the 'shape factor' for the DSD. The larger drops provide the major contribution to total kinetic energy, but occur in relatively small numbers. Using the gamma distribution to represent the DSD instead of the exponential is believed to be more accurate because it is graphically narrower and contains the assumption that there are fewer large drops in the rain.

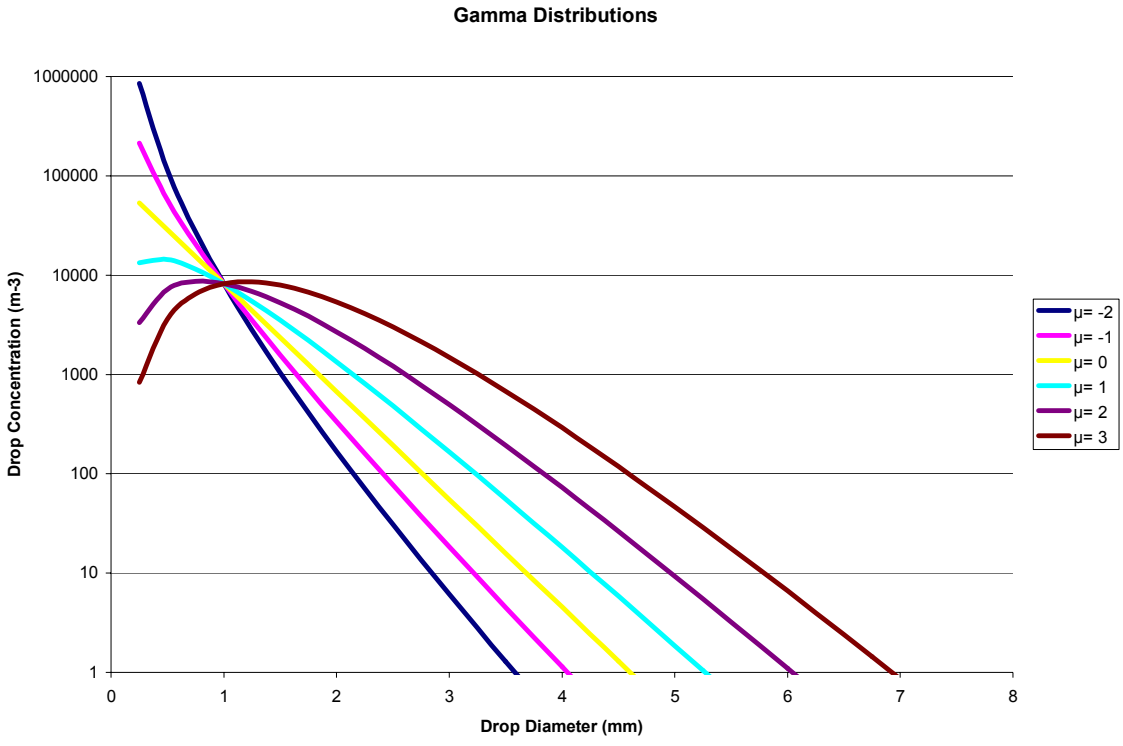

Figure 2.2: Example of statistical gamma distribution with the legend representing different values of μ, with $N_T = 10^5$ drops m^{-3} and $\Lambda = 2.5$ mm^{-1}.

The exponential DSDs imply calculations that are over-estimating the kinetic energy caused by falling rain. It is believed that the Marshall and Palmer (1948) DSD is appropriate for low rainfall rates, but μ increases with rain rate (Fox 2004). The Marshal-Palmer (1948) exponential DSD is a special case of a gamma distribution when μ is 0.

2.3 Kinetic Energy

Soil loss from interrill erosion during rainfall events is a function of rainfall kinetic energy. For equal soil conditions, the greatest soil erosion is associated with the larger raindrops and greater rainfall intensities. Larger drops have both larger mass and greater terminal velocities, and therefore will have greater kinetic energy. Since the greater kinetic energy rainfall occurs with convective type storms, an alteration to the Marshall and Palmer (1948) method may need to be explored.

Rainstorm intensity can be measured directly with a rain gauge, with rainstorm energy as a function of mass and terminal velocity of raindrops. The latter is relatively difficult to determine compared to rainstorm intensity. Typically, rainstorm energy is calculated based on measurements of the relation between rainstorm intensity, DSD, and raindrop velocity (Renard *et al*. 1997).

Since soil loss is a function of rainfall kinetic energy, a relationship of raindrop DSDs to kinetic energy must be established. First, kinetic energy (KE in joules) is defined as

$$KE = \frac{1}{2} m v^2 \tag{2.5}$$

where *v* is the velocity of the drop, and m is the mass of the drop, as a function of raindrop diameter given by:

$$m(D) = \frac{\pi}{6} \rho D^3 \tag{2.6}$$

and ρ is the density of water. From this expression, rainfall rate can be determined by incorporating terminal velocity of the raindrops as a function of raindrop size, *v*(D), in m s^{-1}. This rainfall rate calculated from the gamma parameters μ, N_T, and Λ, is given by

$$R_G = \frac{\pi}{6} \int N(D) D^3 v(D) dD \tag{2.7}$$

Since raindrop energy flux (the transfer of kinetic energy from the raindrop to a surface) is the variable of greatest interest for soil erosion studies, the following relationship is used:

$$KE_G = \frac{\pi \rho}{6} \int N(D) D^3 \left[v(D) \right]^3 dD \tag{2.8}$$

In this thesis, the relationship from Ulbrich (1983) for *v*(D) (m s^{-1}) will be used:

$$v(D) = 3.78 D^{0.67} \tag{2.9}$$

since this method has been shown to be accurate for a wide range of

raindrop sizes (drops of 0.5 to 5.0 mm diameter having theoretical terminal velocities of 2.4 to 11.1 m s^{-1}, respectively), making calculations straightforward (and less complicated) (Fox 2004). Another example of theoretical empirical relationships of terminal drop velocity includes the fall velocity from Atlas and Ulbrich (1977). This relationship is shown by

$$v(D) = 3.87D^{0.67} \tag{2.10}$$

A more complicated terminal velocity relationship from Beard (1985) is shown by

$$v(D) = v_0\left(\frac{\rho_0}{\rho}\right)^m \tag{2.11}$$

where ρ_0 is 1.194 kg m^{-3}, and ρ the air density (kg m^{-3}) in proximity. Equations (2.12) and (2.13) below show the relationships of m and v_0

$$m = 0.375 + 0.025D \tag{2.12}$$

$$v_0 = e^{\left(B_0 + B_1X + B_2X^2 + B_3X^3\right)} \tag{2.13}$$

with X=ln(D), B= 5.984, B_1= 0.8515, B_2= -0.1554, and B_3= -0.03274.

Substituting equations (2.3) and (2.9) into (2.8), results in the following:

$$KE_G = 3.78^3\,\frac{\pi\rho}{6}N_T\int D^{\mu+5}e^{(-\Lambda D)}dD \tag{2.14}$$

One can complete the integral using the following solution

$$\int D^n e^{(-aD)}dD = \frac{\Gamma(n+1)}{a^{(n+1)}} \tag{2.15}$$

where n is μ+5 and a is Λ. Then, kinetic energy flux (KE_G) can be calculated by

$$KE_G = 3.78^3 \frac{\pi\rho}{6} N_T \frac{\Gamma(\mu+6)}{\Lambda^{(\mu+6)}} \tag{2.16}$$

and using the same methods with equation (2.7) gives a function for rainfall rate

$$R_G = 3.78 \frac{\pi}{6} N_T \frac{\Gamma(\mu+4.67)}{\Lambda^{(\mu+4.67)}} \tag{2.17}$$

Kinetic energy flux and rainfall rates are now expressed as functions of the parameters of the DSD.

While much of the energy required to generate soil erosion is derived from raindrop impact, soil loss is greatest when runoff occurs from rill and interrill erosion. The raindrop kinetic energy is less effectively used in generating soil loss when runoff is absent than when runoff is already occurring. The efficiency by which the energy of raindrop impact is utilized varies with the depths and velocities of the surface runoff flow (Kinnell 1983).

2.3.1 Horizontal Wind Component and Kinetic Energy

There are other contributions to raindrop fall velocity. Some have emphasized the significance of wind speed on drop velocity and storm kinetic energy (Laws and Parsons 1943; Wishmeier and Smith

1958), but have not incorporated the effect of wind speed on the drop velocity. Wind speed affects storm kinetic energy by determining the angle at which the raindrops impact the soil surface. Soil surface roughness and surface gradient determine the distribution angles of droplet impact and influence the relation between the normal and tangential impact forces (Helming *et al.* 1993) in the case of vertically falling rain. Introducing a horizontal component to raindrop fall velocity changes the impact angle of the droplets, affecting the normal components of the droplet impact forces relative to the soil surface making modeling of the impact problematic. The impact of wind accounts for approximately one fourth of the total kinetic energy within rainstorm events (Helming 2001).

It is shown that increased kinetic energy of raindrops due to prevalent wind direction can be computed, and can explain outliers in a correlation diagram between soil loss and kinetic energy. However, one must know the slope aspect to the wind (Pedersen and Hasholt 1995). Also, highly erosive rainfall intensities generally coincide with the peak wind velocities (Aina *et al*. 1977). From natural rain field experiments, soil erosion caused by the actual displacement of soil by the wind itself after being displaced by the raindrop impact or splash does occur. However, more research is needed to better quantify this aspect of soil erosion (De Lima *et al*. 1992).

The inclusion of the horizontal wind component, *u*, in to the previous form of kinetic energy flux (2.16) from Fox (2004) is shown by

$$KE_{TG} = \frac{\pi\rho}{6}\int N(D)D^3\left[v(D)\right]^3 dD + \frac{\pi\rho}{6}\int N(D)D^3u^2v(D)dD \qquad (2.18)$$

where KE_{TG} is the total kinetic energy flux. Completing the integrals, and substituting (2.16) and (2.17), we get a simpler form for KE_{TG}

$$KE_{TG} = KE_G + u^2\rho R_G \qquad (2.19)$$

The Helming (2001) kinetic energy formulation was determined by

$$KE_T = 0.5R\left(v(D)^2 + u^2\right) \qquad (2.20)$$

where v(D) is the terminal velocity (m s^{-1}) of a raindrop, and u is the wind velocity (m s^{-1}). This formulation incorporates different DSDs in v(D), along with horizontal wind velocity u.

2.4 Rainfall Simulators

Soil erosion research has historically used one of three methods of forming raindrops via rainfall simulators. One of the first was hanging yarn simulators use a water spray applied to cloth draped across chicken wire. When the water causes depressions in the cloth in the chicken wire openings, the water travels down the hanging yarn strands forming drops (Parsons 1943). Using this method, drop size

was controlled by yarn size and limited to drops less than about 4 mm (Bisal 1960).

Tubing tips are a more precise method of forming simulated raindrops. This method requires submerging tubes (of various types depending on simulator) in tanks of water, and allowing drops to fall 10.7-12.2 m to reach at least 95 percent of the terminal fall velocity. Compared to hanging yarn simulators, tube simulators have a wider range of drop sizes at greater precision.

Nozzle simulators use a nozzle or drop former, and a mechanism to apply the desired spray pattern. The nozzle forms drops with initial velocity governed by the pressure applied to the nozzle, allowing for less fall time to reach terminal velocity. The governing characteristic of this simulation method is the nozzle, which typically creates flow rates that are too intense and median drop sizes that are too small (Mutchler and Hermsmeier 1965). Desirable characteristics of rainfall simulating equipment include (Meyer 1965):

- Drop-size distribution and fall velocities near those of natural rainfall at comparable intensities
- Intensities in the range of storms producing medium to high rates of runoff and erosion

- Application area of sufficient size for satisfactory representation of treatments and erosion conditions to encompass "real field" conditions
- Uniformity of intensity and drop characteristics throughout the study area
- Rainfall application nearly continuous throughout the study area
- Angle of impact not greatly different from vertical for most drops
- Accurate reproduction of storms

While all these characteristics are ideal for simulating rainfall, some of those characteristics mentioned by Meyer (1965) will probably not accurately represent convective type storm events, such as uniformity of rainfall intensity and angle of impact nearly vertical. A portion of the results of this thesis will present the difficulties in mimicking natural rainfall when dealing with convective, high energy rainstorms.

It has been shown in laboratory simulations that greater infiltration rates occur when the rainfall intensities are lower. According to Thompson and James (1985), when determining the effect of water droplet impact on the infiltration capacity of known soil, the maximum depth of water infiltrated prior to ponding occurred at

the smallest application intensity (30 mm h^{-1}) used in the test of 30, 50, 100, and 150 mm h^{-1}. The depth of infiltration increased as kinetic energy in the form shown in (2.21) (Stillmunkes *et al.* 1982) decreased.

$$KE = \frac{\rho_W}{2} At(V_{di})^2 \tag{2.21}$$

where A is the application rate (m s^{-1}), t is the exposure time (s), ρ_w is the density of water (kg m^{-3}), and v_{di} the droplet impact velocity (m s^{-1}).

This chapter has presented the problem that previous work has yet to clearly solve regarding accurately representing natural rainfall via numerical modeling and indoor simulations of such rainfall. DSD methods were described, presenting their strengths and weaknesses. The methodology section of this thesis will describe in greater detail how the gamma DSD technique will be analyzed, and how the data were collected given the known problems and inconsistencies that may present themselves during the analysis.

Chapter 3

Methodology

3.1 Equipment and Facilities

The equipment used in this project consisted of various devices operated at the facilities associated with the University of Missouri-Columbia. Field data for natural rainfall events was gathered using the Atmospheric and Climatic Experiment Station (ACES) located southeast of the city of Columbia, MO, where various hydro-meteorological instruments are in use. Simulated rainfall data were collected using the indoor rainfall simulator located on campus in the Hydrology Laboratory of the Agriculture Engineering Building. These facilities and the equipment used in this project (described in greater detail later in this chapter) allowed for in-situ measurements for data collection of various natural rainfall events and multiple laboratory tests using tools that were readily available. This also allowed independent control when governing the type of data and methods necessary for this project, rather than relying on pre-existing data from outside sources. Having the ability to customize the data collection techniques and methods increased the flexibility available to

deal with troubleshooting and the nature of the rainfall events that are common to the Central Missouri region.

3.1.1 Atmospheric and Climatic Experiment Station

A vital component to this thesis is the Atmospheric and Climatic Experiment Station (ACES) at the University of Missouri's South Farm Field Research Center located southeast of the city of Columbia, MO (shown by the red star in figure 3.1). This facility contains a variety of equipment ranging from the Missouri Climate Center's Campbell Scientific weather station, to the local NBC affiliate's (KOMU) retired Doppler radar.

Specific to this research are two tipping bucket rain gauges, anemometers and wind vanes at various heights, soil beds, and a Rain Imaging System (RIS) containing a video disdrometer. The rain gauges operate at 0.01 inch (0.254 mm) catchment intervals at each tip of the bucket. Data collection for these gauges is archived in two-minute recording intervals, every 10 minutes. One rain gauge was located in close proximity to the video disdrometer, approximately 1 m above ground level (AGL), with the other gauge atop the ACES building, about 4 m AGL. The anemometers and wind vanes utilized in this project at the ACES facility existed at heights of 0.75, 1.5, and

10 m AGL. The 3 m AGL wind instruments located on the Missouri Climate Center's weather station were not included here due to the differing data recording intervals relative to the three other heights.

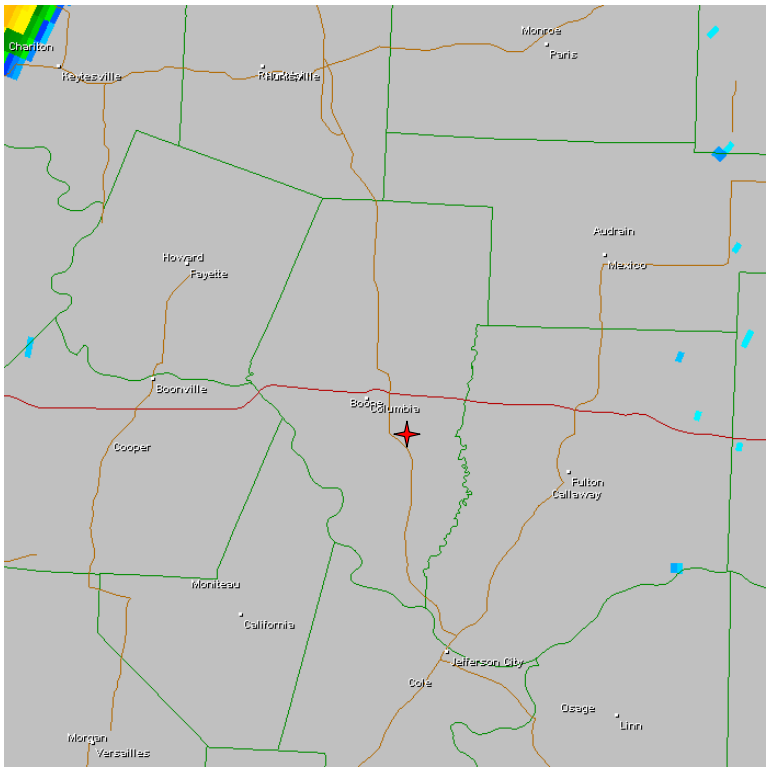

Figure 3.1: Depiction of the location of South Farm ACES by the red star.

3.1.2 Rainfall Simulator

The simulated rainfall data were gathered from a tubing-tip simulator located in the hydrology lab in the Agriculture Engineering Building at the University of Missouri. This system simulates natural rainfall by varying rainfall rates and DSDs independently of each other.

Drops were allowed to fall from a height within the tower of 14 m, allowing for drops of 4.3 mm and smaller to reach 95% of their terminal velocity (Regmi and Thompson 2000).

Data for this study were gathered using a fixed rainfall rate, and only DSDs were allowed to vary. The DSD did not vary significantly by changing the rainfall rates, but by varying the screen suspension height. The drop redistribution screen (part of the schematic in figure 3.2) is designed to break up the initial drops falling from the dripper tank, then impacting the screen at varying distances below the tank, allowing DSDs to vary, particularly median drop size diameter D_0.

3.1.3 Rain Imaging System

Without any method of gathering data regarding the size of the raindrops, the hypotheses presented in chapter 1 could not be tested. The Rain Imaging System (RIS) used in DSD data collection was on loan from the University of North Dakota's School of Aerospace Engineering, Atmospheric Sciences branch. The RIS contains three main hardware components; a flood lamp, PC, and the camera and housing. The RIS camera (shown in figure 3.3) has several important features including a 32 mm by 24 mm focal area, 60 frames s^{-1} video capture, camera shutter speed of 1/80,000 s, and the software features high-speed image compression for long term deployment.

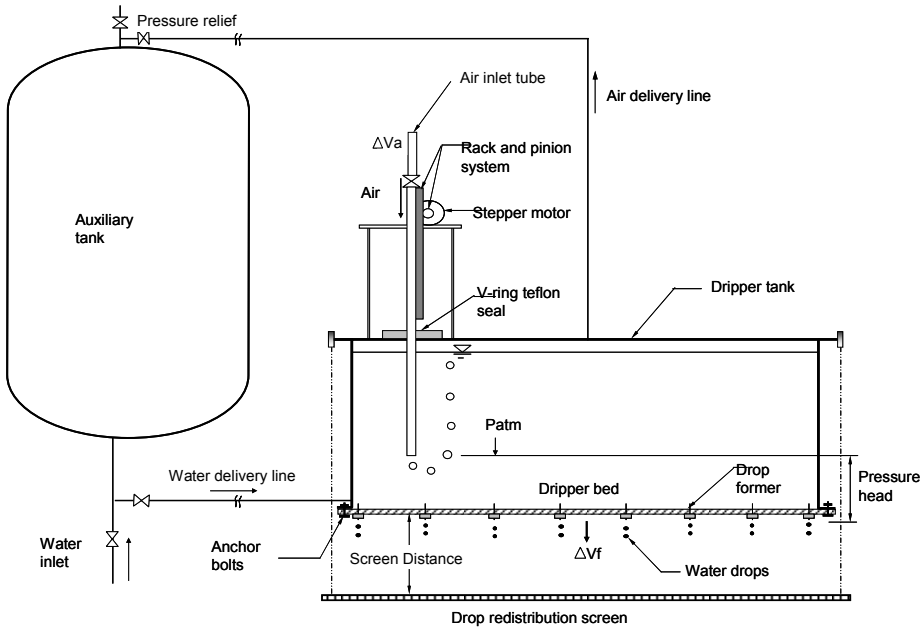

Figure 3.2: Schematic of indoor rainfall simulator used in this thesis (from Regmi and Thompson (2000)).

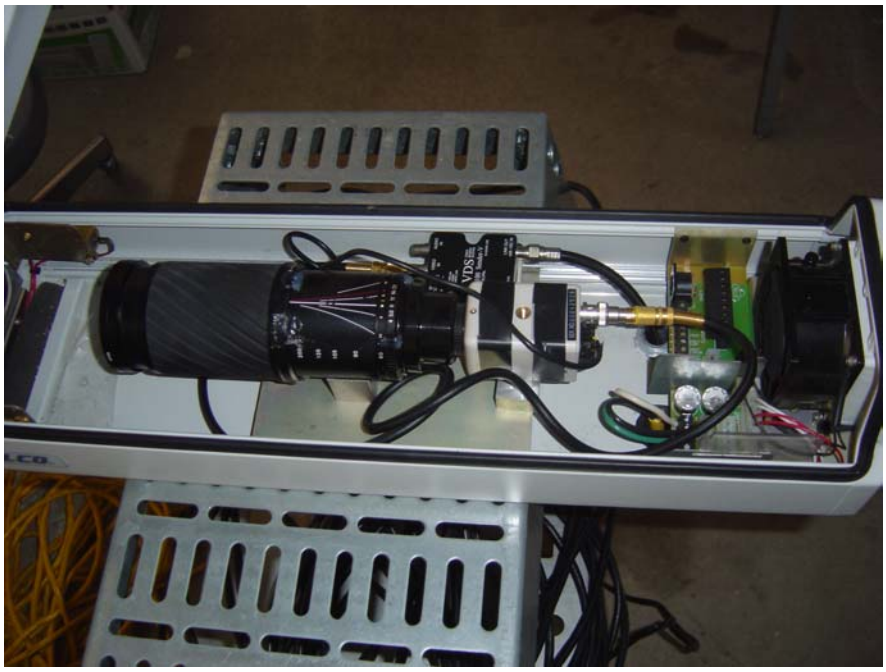

Figure 3.3: Image of the camera component of the RIS.

The depth of the field of view is controlled by pattern recognition software written specifically for the RIS. This software is used to select those drops that appear in the sampling volume for processing. This is accomplished by a "bright spot" feature that appears in those drops that are in the proper field of view. This feature is evident in the raindrop images in figure 3.4. If the drop is in the measurement volume, the drop contains a light-colored, hole-like spot or "bright spot" within the drop outline. Drops outside the measurement volume contain no hole. The drops more than a few centimeters outside the

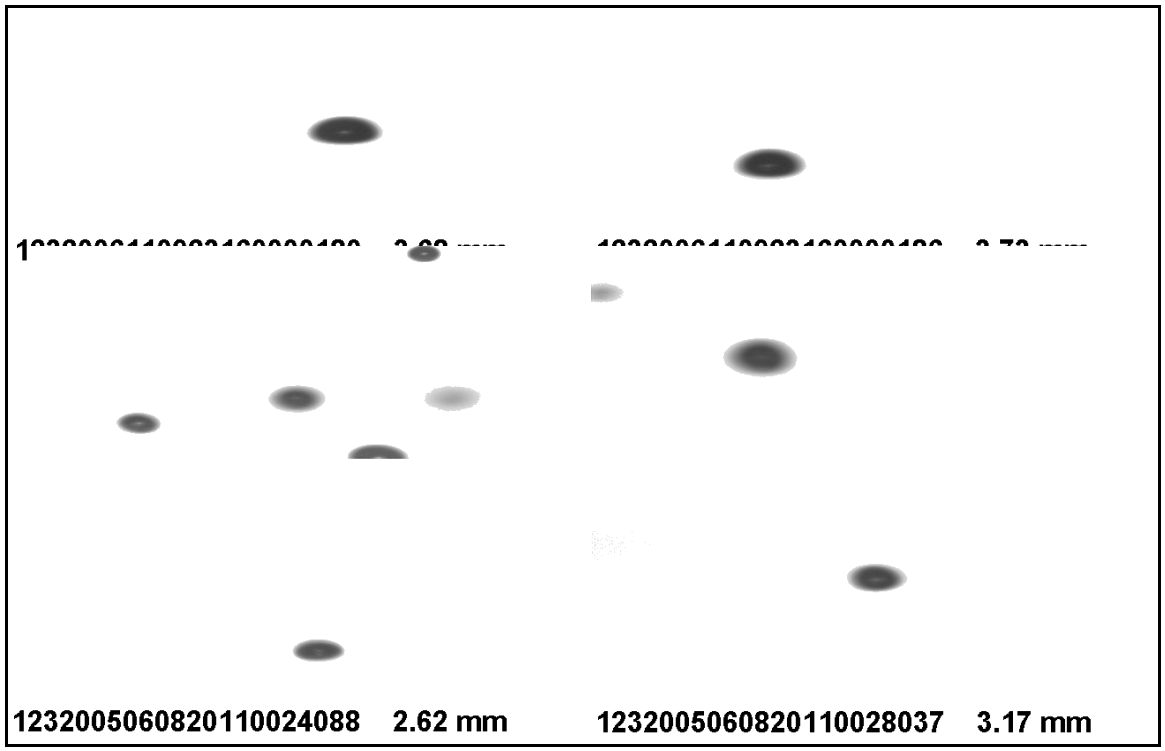

Figure 3.4: Images of raindrops from the RIS.

measurement volume are too faint for data processing, and, for quality control purposes, are ignored using this software. This focal volume is located approximately 2 m from the lens, consisting of a 32 mm wide x 24 mm tall focal plane.

The flood lamp contains a 300 watt halogen bulb that is used to focus the camera, allowing the raindrops to generate a shadow as they pass through the measurement volume. This shadow is the data the processing software digitally analyzes, providing the DSD data used in this thesis. When rainfall events were anticipated, the flood lamp and camera were set up in the field as shown in figure 3.5, approximately 3 m (10 ft) apart, the predetermined distance for optimum performance of the RIS. The post-processing software contained on the PC draws an outline around those rain drops with the bright spot, gathering drop specific information such as major and minor axis length and raindrop area.

3.1.4 Soil Beds

Quantifying soil loss in natural rain events was attempted using soil beds designed in-house at the MU Agriculture Engineering facilities. Two designs were used over the duration of the project described in this thesis. The first set of beds were pre-existing soil

Figure 3.5: Image showing deployment of the RIS outdoor components at the ACES.

beds, used in various other projects within the Agriculture Engineering facility, with dimensions 0.20 m deep, 0.30 m wide, and 0.50 m in length. These soil beds were abandoned due to complications in regard to soil wetting that arose during the summer 2005. These complications will be explained in more detail in the results section. The new soil beds (figure 3.6) were designed with dimensions of width and length identical to the pre-existing beds, but with a decreased depth of 0.15 m. This minimized the distance between the surface of the soil and the lip of the bed to 0.01 m to increase exposure to the rainfall.

The soil beds were packed using a depth of 0.05 m of coarse

sand beneath 0.10 m of evenly compacted, dried Mexico silt loam soil. No pre-wetting was done in this project, but may be a suggestion for future projects that will be proposed in the future work section of chapter 6. In the field, three soil beds were used, initially set side-by-side, facing in the same direction. A predetermined slope of 3% was used for correlation to ongoing work in the Hydrology Laboratory containing the indoor rainfall simulator. Later trials were tested with each soil bed set up at a 90° different orientation relative to each other tray. The soil beds were sloped downward towards the southeast, northeast, and northwest compared to the initial setup in which they were sloping downward facing the northwest. This was done to test a hypothesis that the effects of wind and impact angle may have limited our ability to capture soil-loss data during natural rainfall soil wetting using these particular soil beds.

3.2 Data

All data analyzed in this study were gathered first-hand from in-situ observations collected from either the ACES or the Hydrology Laboratory. Natural rainfall events included the full range of data collection, including RIS data, rain gauge data, and wind data from all three levels. The laboratory or simulated rainfall events did not include wind data due to obvious limitations of an indoor rainfall simulator.

These two components of this study will be compared and contrasted with one another, as well as related to previous work regarding this specific aspect of soil erosion.

3.2.1 Natural Rainfall Events

The natural rainfall DSDs were gathered using the RIS at the ACES during various natural rainfall events ranging from severe weather, high precipitation cases, to lighter rainfall scenarios where runoff potential was small. The severe, large precipitation samples, or those containing high rainstorm energy potential, generally created environments where some aspects of the project were unable to be safely monitored and data properly collected. That is, the conditions that accompanied a few of the rainfall events prevented one from accurately monitoring, and properly collecting, soil loss data due to the frequency of lightning flashes, strong winds, or large hail. The rainfall events presented here are separated into two different categories: category I and II. Category I events are those events characterized by light rainfall, or those scenarios where soil runoff was not evident or not expected. Category II events are characterized by high intensity rainfall, specifically those where runoff occurred and rainfall rates remained high.

Figure 3.6: The soil beds used in attempting to gather soil loss data, located at the ACES.

These events can also be compared to laboratory studies, since rainfall rates in the indoor simulator are limited to approximately 35 mm h^{-1} and greater. A radar image, shown in figure 3.7, is an example of a category II event. Notice the higher reflectivities representing heavy rainfall and/or hail. These scenarios are of greatest interest because of the great kinetic energy potential from large raindrops and from

greater potential for high horizontal wind velocities.

For a more direct comparison to the simulated rainfall, the time intervals of the given rainfall events were shortened to relate to the datasets gathered from the simulated rainfall. Specifically, simulated rainfall data were gathered in a maximum of 10 minute intervals. So, while the natural rainfall event durations varied greatly, the natural rainfall data were broken up into smaller intervals to match those of the simulated rainfall, 10 minutes during the most intense portion of the storm. The wind and rain gauge data were also used in a corresponding manner. Otherwise, the drop concentration, N(D), would be much greater in natural events compared to simulated rainfall, and direct comparisons may be less accurate.

3.2.2 Simulated Rainfall

Simulated rainfall datasets were gathered in 10 minute intervals at a preset rainfall rate. The rainfall rate was controlled by the position of the air inlet tube above the dripper tubes. Rainfall rates were similar to the natural category II events the equipment allowed. Figure 3.8 shows the RIS set up prior to data collection in the Hydrology Laboratory. DSDs were varied by adjusting the screen distance beneath the drippers of the water tank.

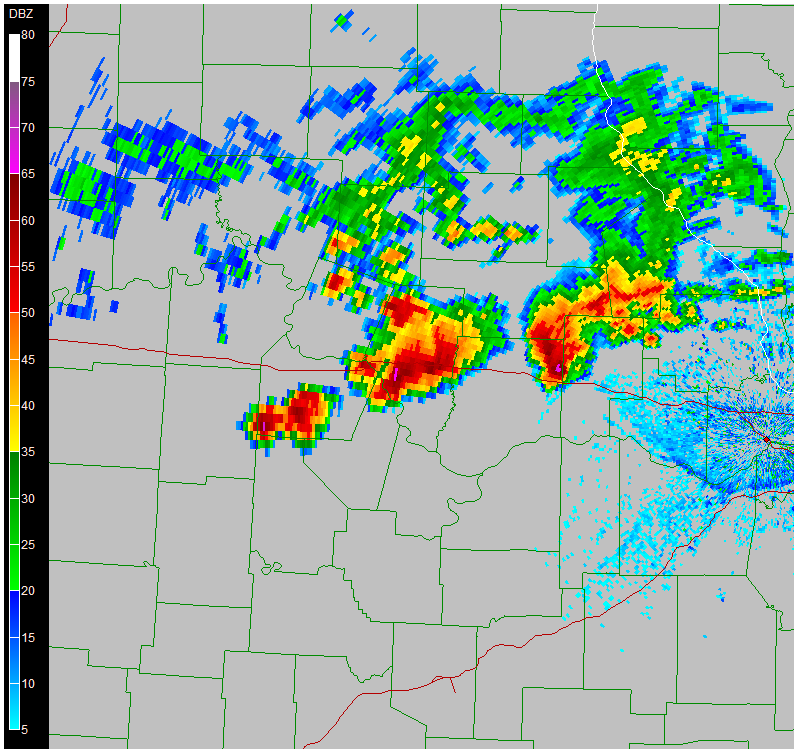

Figure 3.7: Radar image from Saint Louis National Weather Service WSR-88D Doppler radar (KLSX) from 10 June 2006 at 2301 UTC depicting a category II rainfall event.

When the drops exit the drippers, they begin to fall gaining kinetic energy before impacting this screen. On impact, the drops break into different sizes beneath the screen. When the screen is at larger distances, the drops have a greater initial velocity and kinetic energy that allow the drops to break up into a larger number of drops beneath the screen, creating a larger concentration of drops of smaller diameters, decreasing D_0. However, when the screen is at a shorter distance beneath the drippers, less kinetic energy is attained prior to drop impact, allowing for a larger concentration for drops of relatively

large diameters, increasing D_0. Figure 3.9 depicts the vertical extent of the rainfall simulator viewed from below.

3.2.3 Procedure

Rain DSD data from both the natural rainfall events and the simulated rainfall were analyzed using the gamma distribution technique from Testud *et al*. (2001). Graphical and quantitative comparisons were made of the two scenarios to see how well the simulated raindrops can compare to natural rain events using this equipment.

Each rainfall event was categorized either I or II by analyzing rain gauge data, soil loss data (if available), and radar imagery. From here, raindrop data was processed to produce DSDs from the gamma distribution method from Testud *et al*. (2001). At this point, an initial graphical analysis was completed to visually compare natural to simulated rainfall. Next, a quantitative analysis of the gamma distribution parameters, discussed in chapter 2, was completed to calculate rainfall rates and kinetic energy. Those parameters include Λ, μ, and N_T. Those rainfall rates were compared to the observed rainfall rates and those rainfall rates calculated from the summation of the drop diameters. This was done for both natural and simulated rainfall events.

Figure 3.8: Deployment of the RIS in the Hydrology Laboratory where simulated raindrop data was gathered.

Figure 3.9: View looking upward showing the vertical extent of the indoor rainfall simulator located in the Hydrology Laboratory.

Two different methods were used in these rainfall rate calculations to test the accuracy of techniques used to develop relationships for comparing natural to simulated rain. Once the steps

outlined here are completed, a view of the ability of simulated rainfall to mimic natural rainfall will be presented, and any complications and suggested advancements will be discussed.

Chapter 4

Cases

In this section, a brief description of each rainfall event will be completed for a better understanding of the weather conditions at the ACES and bring forth any complications that may affect the significance of the results presented by each natural rainfall event. As stated in section 3.2.3, the natural rainfall events were separated into two categories. Category I storms are those rainfall events that did not reach rainfall rates necessary for runoff to occur with the soil beds in the field. This can result from conditions where the expected rainfall rates and timing of runoff not reaching the criteria gathered from laboratory experiments, or that the natural events did not produce runoff as a result of other test characteristics. The dates for the five category I events are:

- 13 August 2005
- 25 August 2005
- 26 August 2005
- 31 May 2006
- 14 July 2006

The category II storms are those rainfall events where runoff from the soil beds was noted during natural rainfall experiments. The dates for those two natural rainfall events were 28 September 2005 and 10 June 2006.

4.1 Category I Rainfall Events

The data collected on 13 August 2005 were the first data set that included all of the parameters of this project. All previously gathered data only included rain drop data from the RIS, with no data available from the rain gauges, 1.5 and 0.75 m wind instruments, or soil beds to compare with the DSD data. Figure 4.1 shows a radar reflectivity image taken from the Saint Louis (KLSX) National Weather Service (NWS) Weather Surveillance Radar, 1988 Doppler (WSR-88D) at 2111 UTC. Two different broken lines of convective cells were present, converging near Boone County, close to the ACES. It is important to note the relatively low reflectivities near this location. This likely explains the rainfall rates being smaller than required to generate soil runoff from the soil beds. The time series of observed rainfall rate from the close-proximity rain gauges is shown in figure 4.2. Notice that the duration of the heaviest rainfall rates of between 20 and 35 mm h^{-1} occurred between 2100-2140 UTC.

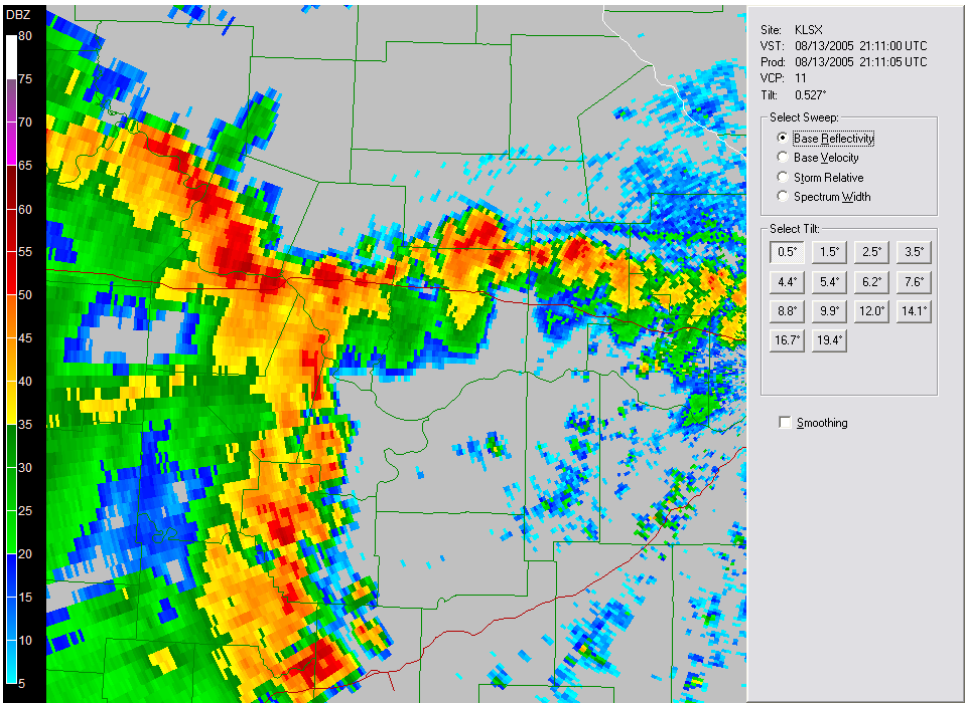

Figure 4.1: Base reflectivity radar image at 2111 UTC on 13 August 2005 from the Saint Louis NWS radar (KLSX).

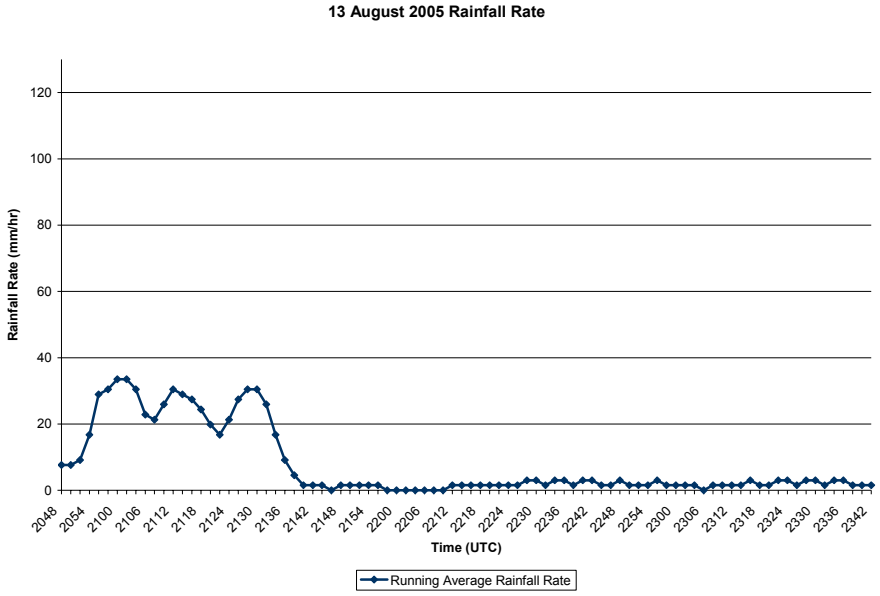

Figure 4.2: Time series of rainfall rates on 13 August 2005 from 2048-2342 UTC.

It will be discussed later in this section which specific 10-minute time periods were used in the DSD analysis and the reasoning behind the choice of such a short time interval.

Figure 4.3 depicts the radar reflectivity from the rainfall event on 25 August 2005. Notice the more widespread nature of the precipitation, with a few embedded convective cells to the south and east-northeast of the ACES. This rainfall event resulted in the least intense rainfall rates of the useful data sets. The rainfall rates never exceeded 10 mm h^{-1} (figure 4.4) throughout the time data were being collected. The duration of the event was approximately 80 minutes, with the greatest intensity rainfall of 6 mm h^{-1} occurring between 1136-1208 UTC.

The following day, 26 August 2005, the next data set was collected after 1200 UTC. Figure 4.5 shows the first of two convective cells that produced the most intense rainfall. Notice the embedded areas of intense convection within the parent line convective cells. Two areas of convection passed over the ACES allowing for two separate rainfall data sets, both of which will be discussed. Although figure 4.6 shows three individual peaks in rainfall intensity, the focus will be on the first and last peak due to a gap in RIS data due to a brief power

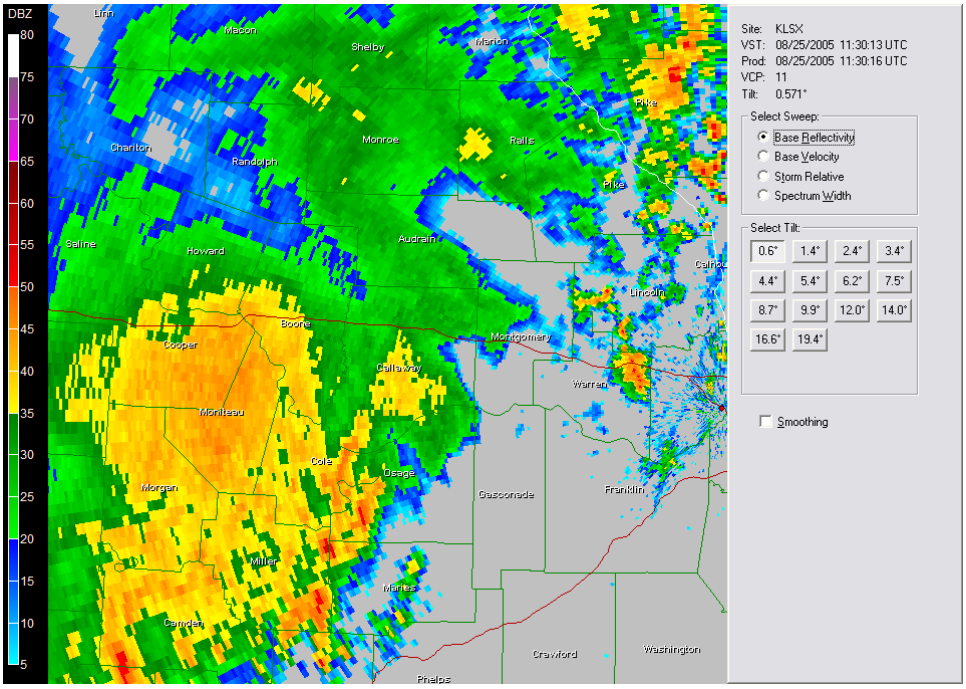

Figure 4.3: Base reflectivity radar image at 1130 UTC on 25 August 2005.

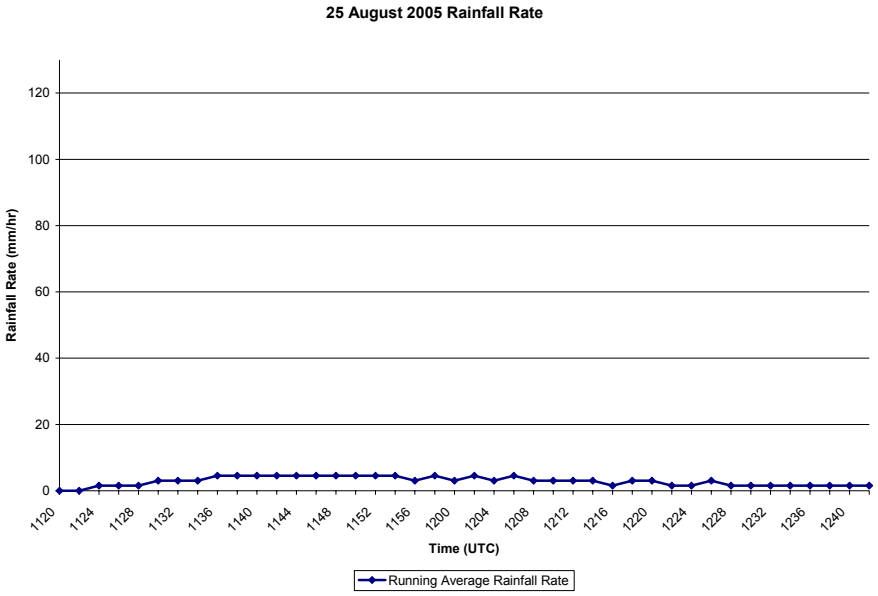

Figure 4.4: Time series of rainfall rates on 25 August 2005 from 1120-1242 UTC.

outage caused by lightning. This issue will be discussed later in more detail, as lightning and other dangerous weather aspects created some difficulties during the entire project.

The first set of data analyzed on this day occurred from about 1210-1300 UTC, when the rainfall intensity peaked around 35 mm h^{-1}. The second data set was collected from 1430-1450 UTC, with a slightly lesser maximum rainfall rate of about 25 mm h^{-1}. It is important to notice the sharp peaks in rainfall intensities, as this signifies the high variability in rainfall intensity, another difficulty that was evident when attempting to capture soil loss data from the soil beds. Again this issue will be discussed later in more detail.

The next rainfall event occurred on 31 May 2006. This event collected rainfall data that fell from convective rainfall that developed in the vicinity of the ACES. This is evident in figure 4.7, where the radar reflectivity image shows convective cells located directly overhead of the location of the ACES, with the lack of additional development to the west and northwest. The data collected by the RIS was collected after 2320 UTC, at which time the longer duration of relatively heavy rainfall occurred this day. Figure 2.8 shows the highest rainfall rates fell between 2324-2334 UTC, when the rainfall rates peaked near 35 mm h^{-1}, and decreased to around 10 mm h^{-1} after that time.

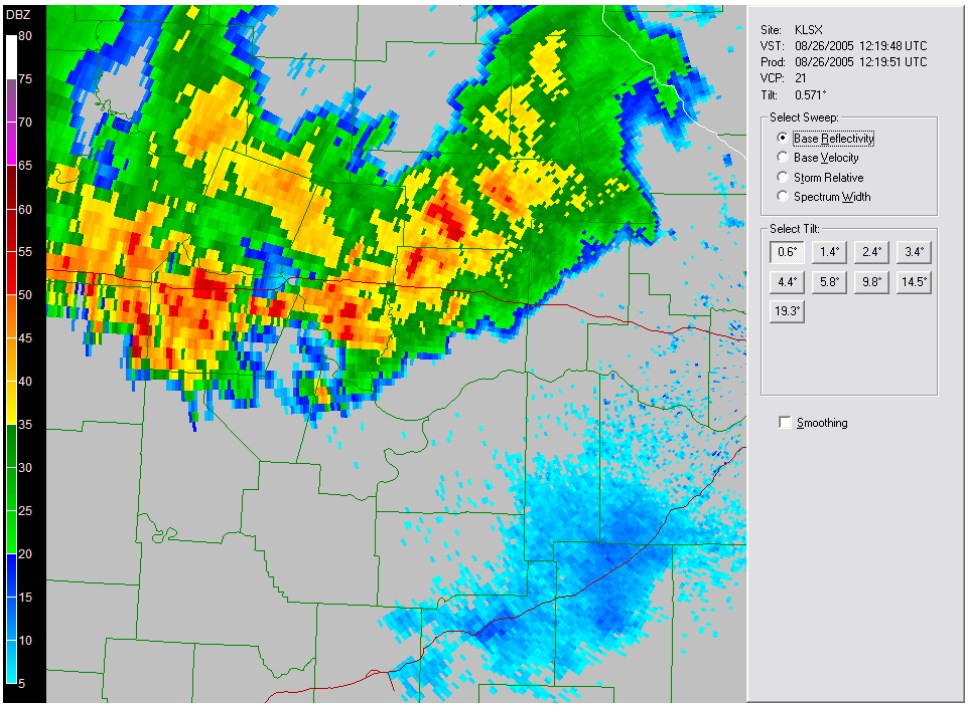

Figure 4.5: Base reflectivity radar image at 1219 UTC on 26 August 2005.

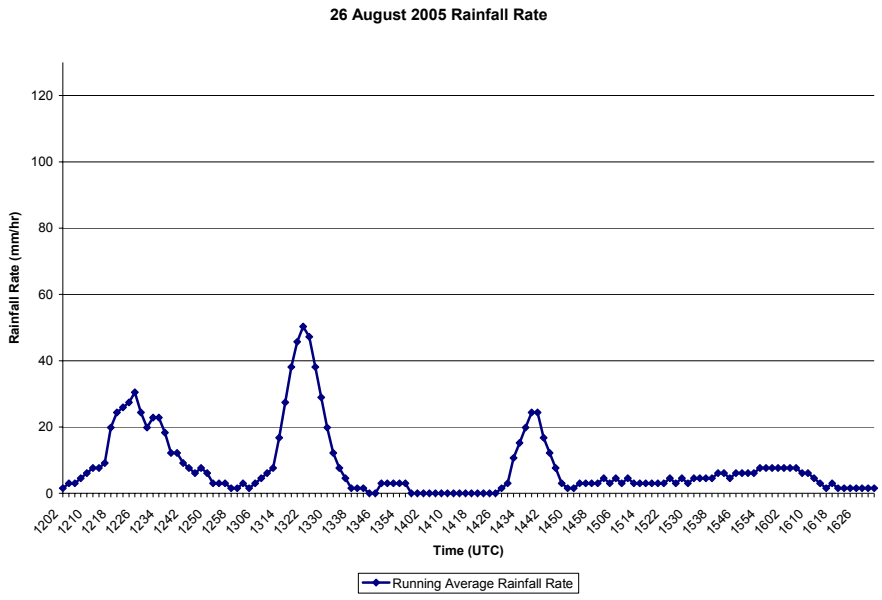

Figure 4.6: Time series of rainfall rates on 26 August 2005 from 1202-1632 UTC.

Also, the sporadic nature of the convection is evidence of the less dynamically active atmosphere, a common occurrence during this experiment. Some of the category I rainfall events were captured on days where the majority of the convection was of the ordinary thunderstorm variety caused by daytime heating, or other smaller-scale influences during the early morning hours. Other rainfall events not discussed in this thesis were ignored because of the lack of appropriate data caused by decaying ordinary thunderstorms near the ACES that did not persist as long as expected.

The final category I event discussed in this thesis took place on 14 July 2006. This late evening event, depicted in figure 4.9, occurred after 0300 UTC, where the southern edge of convection passed over the ACES site. The largest rainfall intensities near 40 mm h^{-1} occurred between 0306-0320 UTC. This particular event had a longer duration of relatively intense rainfall similar to the 31 May 2006 case, compared to some of the other category I rainfall events discussed. This longer duration is depicted in figure 4.10, after approximately 0300 UTC. Even after the peak in rainfall intensity, the rainfall rates did not fall rapidly to zero, but gradually decreased in intensity until 0400 UTC. This same gradual change in rainfall intensity occurred prior to the peak storm intensity, something that should have been beneficial while attempting to capture soil loss data from the soil beds.

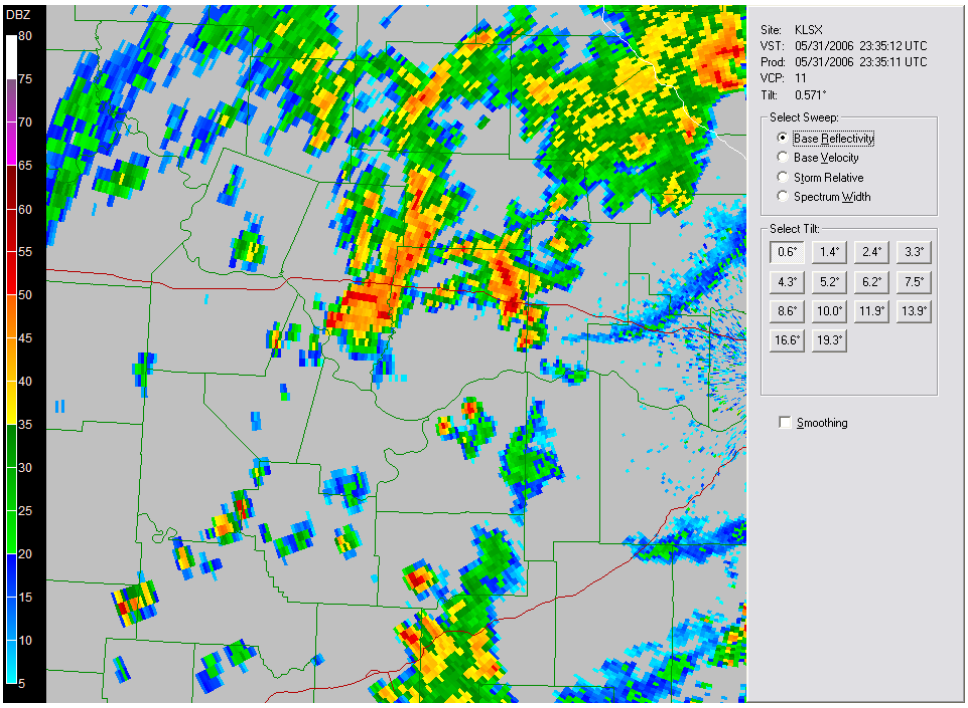

Figure 4.7: Base reflectivity radar image at 2335 UTC on 31 May 2006.

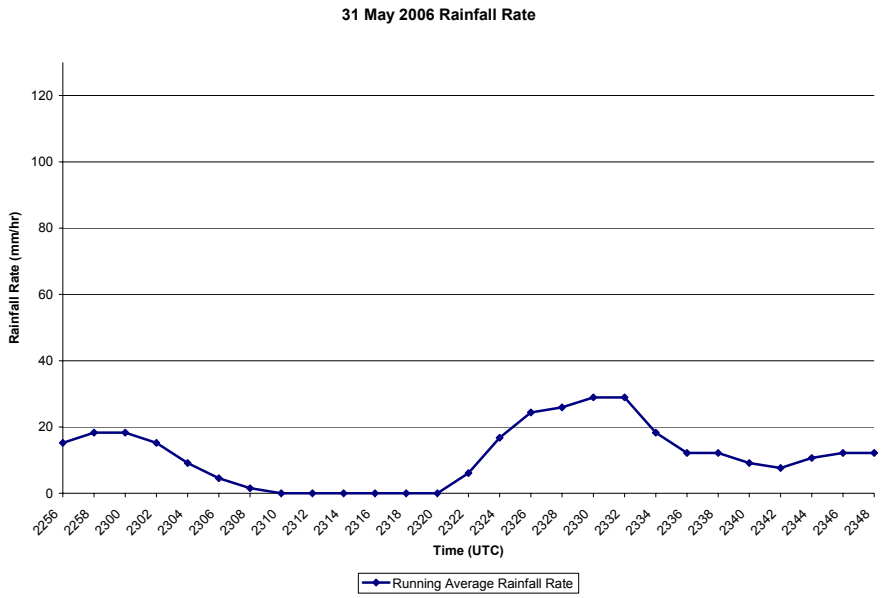

Figure 4.8: Time series of rainfall rates on 31 May 2006 from 2256-2346 UTC.

The category I rainfall events described in this section have all had rainfall intensities that did not exceed 40 mm h^{-1}. None of these events caused observable soil loss from the small dimension prepared soil beds. Controlled studies using similar soil beds in the Agriculture Engineering Hydrology Laboratory have shown some soil loss with rainfall rates near those rainfall rates observed here. However, those studies had controlled, near-constant rainfall rates generated by the rainfall simulator. Also, those simulations did not include any wind influence that may have limited the chances of generating soil loss using the soil beds. The indoor rainfall simulator used is incapable of mimicking wind due to the limitations of the current rainfall simulator.

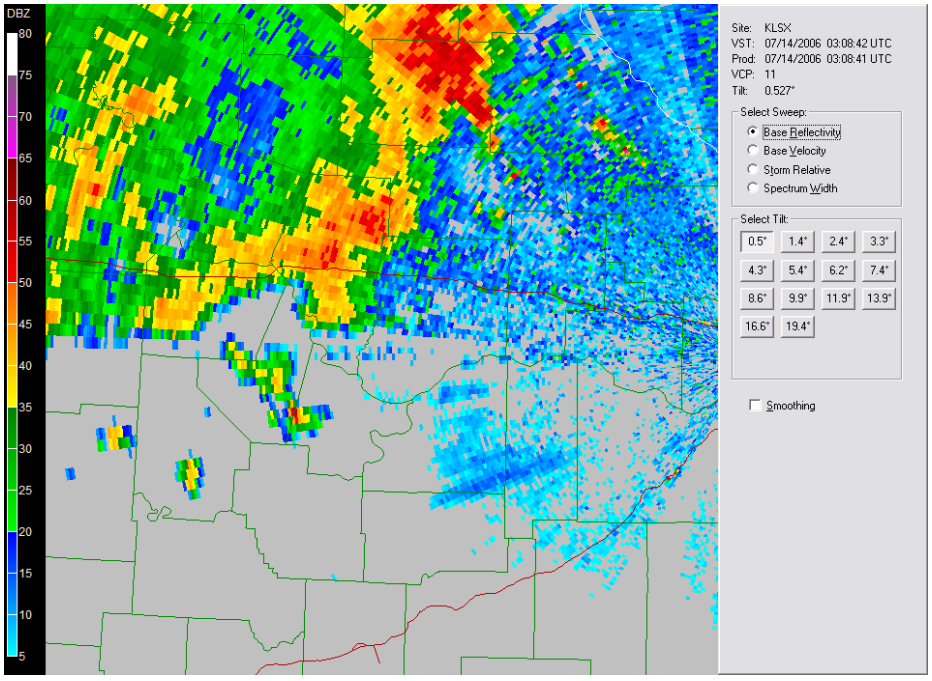

Figure 4.9: Base reflectivity radar image at 0308 UTC on 14 July 2006.

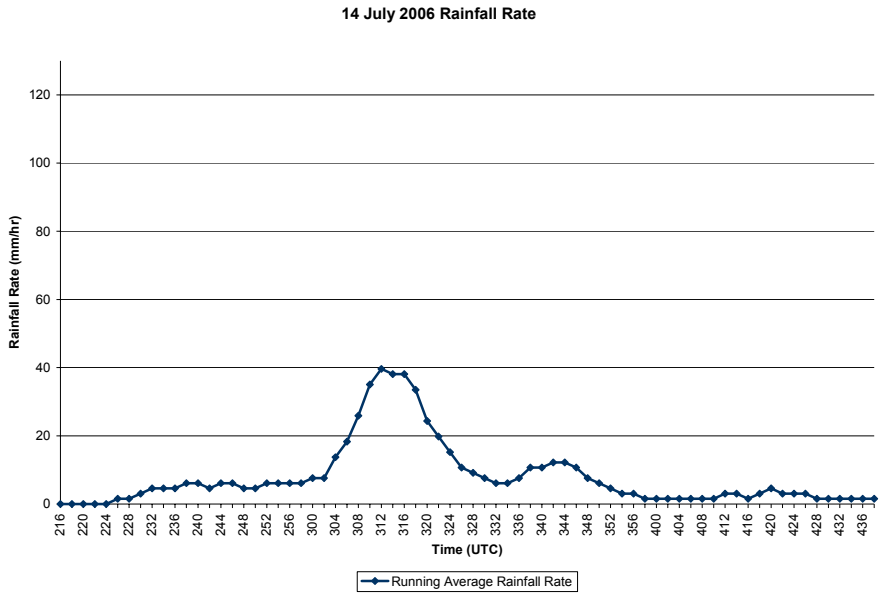

Figure 4.10: Times series of rainfall rates on 14 July 2006 from 0216-0438 UTC.

4.2 Category II Rainfall Events

Those rainfall events in which evident soil loss and/or water pooling was observed were classified as category II rainfall events. These two particular days had convective storm cells that contained greater intensity rainfall rates, and generally persisted in longer duration than the category I rainfall events. The first of rainfall events in this category occurred on the afternoon of 28 September 2005, where strong to severe thunderstorms moved across the ACES from the west, shown in figure 4.11. This event began as an initial high-intensity rainfall rate, then gradually decreased in intensity shortly

thereafter. This is evident in figure 4.12, showing the peak rainfall intensity of about 55 mm h^{-1} that occurred between 1700-1730 UTC.

The final rainfall event discussed in this thesis occurred on 10 June 2006. This event stands out from all other rainfall events in many ways. Firstly, the data gathered during this event occurred during a severe convective storm, which not only contained very heavy rainfall, but included up to quarter-sized (26 mm) hail. Secondly, wind gusts as high as 23 m s^{-1} at 10 m AGL were recorded, which is within 2 m s^{-1} of NWS severe thunderstorm criteria. Figure 4.13 shows the large, high-precipitation (HP) supercell as it moved over the ACES at 1701 UTC, within minutes of the recorded wind gust. It is important to note the size and orientation of this storm, as the direction of movement was important in collecting data during the occurrence of greater intensity rainfall rates over a longer duration than the other events discussed herein. The third and very significant aspect that occurred during this event was evident in the radar image, where the reflectivities exceeded 65 dBZ, which was evidence of the very heavy rainfall and large hail.

Figure 4.14 shows the extent of the rainfall intensity and duration. The initial observation made from this particular rainfall intensity time series is the very great rainfall rates of over 120 mm h^{-1} for natural rain.

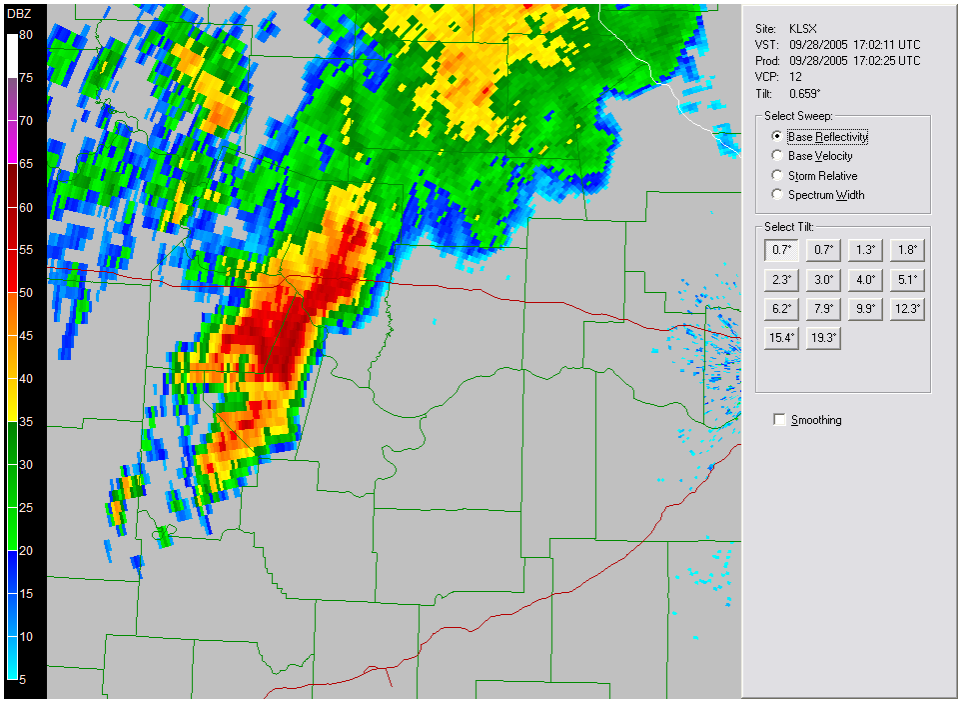

Figure 4.11: Base reflectivity radar image at 1702 UTC on 28 September 2005.

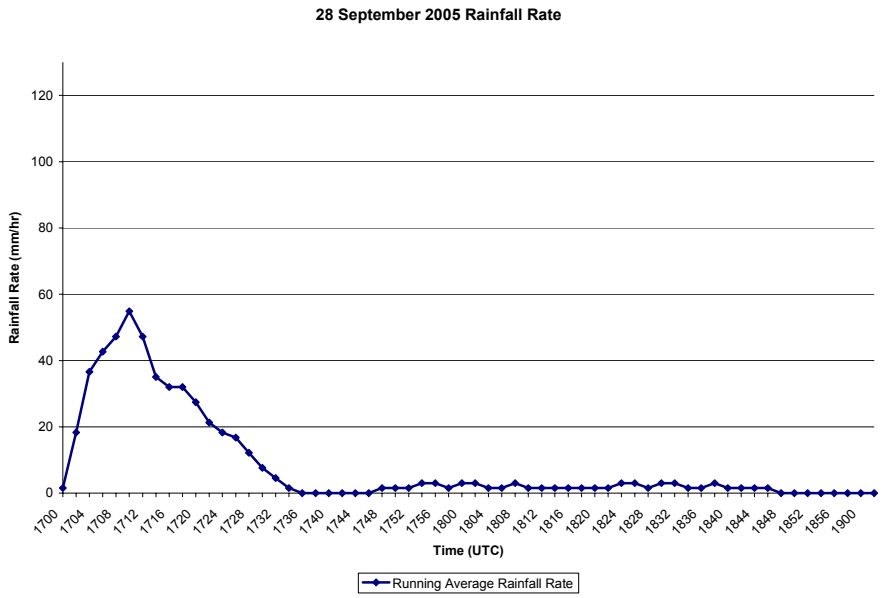

Figure 4.12: Time series of rainfall rates from 28 September 2005 from 1700-1802 UTC.

The other important observation is the duration of the high intensity rainfall, where the rainfall rates exceeded 40 mm h^{-1} from about 2304-2326 UTC. When comparing this rainfall intensity to the others in this study, one can see how extreme this event was, and how much energy some of the most severe rainfall events can contain. It is these types of rainfall events that are likely to cause the most soil loss potential, and are the most difficult to mimic due to the variability in wind-velocities and generating those conditions in a laboratory environment.

In order to complete a more direct comparison of natural rainfall events to the data from the indoor rainfall simulator, the time interval used in the data analysis of natural events was required to be much shorter than the entire duration of the storm. The sample time duration used for gathering data with the rainfall simulator was limited to between 10-15 minutes. This is a limitation caused by the available water in the storage tank of the simulator. A certain level of water is required in order to keep a consistent rainfall rate inline with the empirically derived standards for this simulator. For this study, the natural and simulated rainfall analysis used a 10-minute sample time. The 10-minute duration time that took place during the greatest 10-minute average rainfall intensity was used in all natural rainfall events.

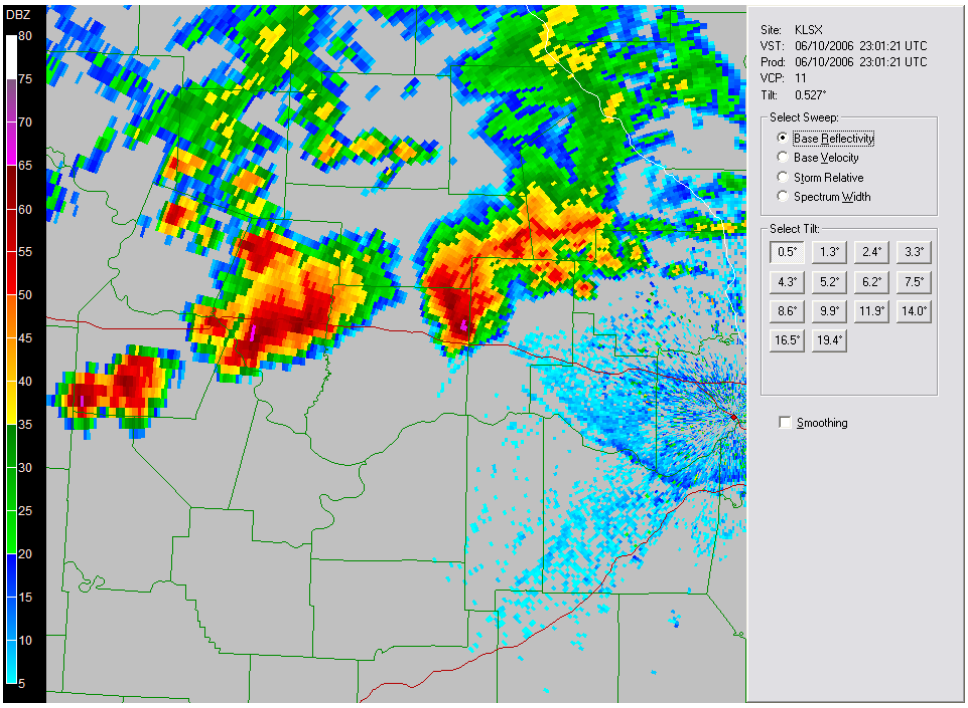

Figure 4.13: Base reflectivity radar image at 2301 UTC on 10 June 2006 from KLSX.

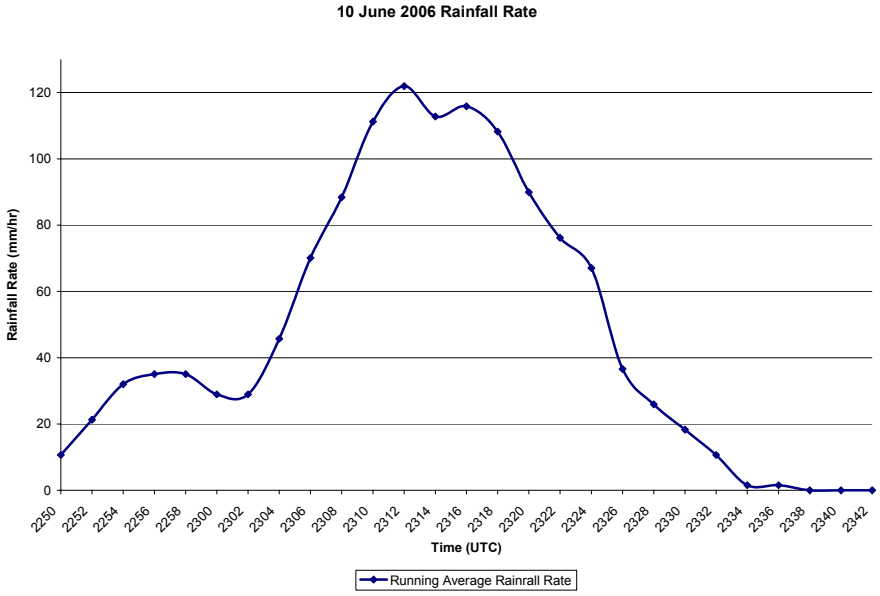

Figure 4.14: Time series of rainfall rates from 10 June 2006 from 2250-2342 UTC.

Tables 4.1 and 4.2 show the selected 10-minute sample time durations corresponding to each rainfall event from the category I and II events respectively. These figures also include the total storm duration, peak rainfall rate (R_P), storm total rainfall, 10-minute average rainfall intensity (R_A), and the 10-minute rainfall accumulation.

Table 4.1: Details of category I rainfall events.

Date	Time (UTC)	Duration (min)	R_P (mm h^{-1})	Total Rain (mm)	Period Examined (UTC)	R_A (mm h^{-1})	Period Total Rain (mm)
13-Aug-05	2048	58	61	18	2100-2110	30	5
25-Aug-05	1124	70	8	4	1140-1150	5	1
26-Aug-05 A	1202	54	61	12	1226-1236	30	6
26-Aug-05 B	1434	114	38	12	1436-1446	21	4
31-May-06	2328	32	53	8	2330-2340	27	5
14-Jul-06	0232	86	61	17	0312-0322	39	7

Table 4.2: Details of category II rainfall events.

Date	Time (UTC)	Duration (min)	R_P (mm h^{-1})	Total Rain (mm)	Period Examined (UTC)	R_A (mm h^{-1})	Period Total Rain (mm)
28-Sep-05	1706	104	99	16	1706-1716	43	8
10-Jun-06	2254	44	152	41	2314-2324	114	23

Chapter 5

Results

This study uses several rainfall events ranging from low intensity rain showers, to extreme, high-energy thunderstorms. For each rainfall event, a graphical comparison of DSDs for the natural events with the DSDs of the indoor rainfall simulator is completed in section 5.1. This analysis was followed by a more in-depth quantitative analysis of the distribution curves fitted to the actual DSDs. Section 5.2 includes the quantitative comparisons involving gamma distribution parameters (N_T, Λ, and μ), actual rainfall intensities (R_A) compared with calculated rainfall rates from both summation of drop diameters (R_S), and gamma-fit curve calculations (R_G). Section 5.2 also presents the results of the kinetic energy flux analysis of vertical falling rain (KE) and the estimated total kinetic energy flux (KE_T). Finally, section 5.3 discusses the soil loss analysis.

5.1 Graphical Analysis

5.1.1 Natural Rainfall Events

Since it is believed that the relatively small concentration of large drops have the greatest influence on soil loss potential, this section focuses on the graphical nature of the observed DSDs. There

are three areas of interest. First, a qualitative analysis of the shape of the DSD plot will be completed, followed by observing the relative concentrations of large and small drop diameters, then finally noting any significant drop sizes that are evident.

The first case in this study occurred on 13 August 2005. Figure 5.1a shows the DSD plots of all natural events with drop concentration N(D) as a function of drop diameter. The first point to notice is the relatively linear shape of the DSD plot on this semi-log graph. This closely resembles the exponential DSD fit proposed by LP/MP. This result is reasonable since this rainfall event was characterized by relatively small intensity rainfall. Table 5.1 shows this intensity, with the average rainfall rate (R_A) during this sample time being 30 mm h^{-1}. The next characteristic of this DSD plot to note is that the maximum observed raindrop diameter is approximately 5 mm. However, there was a small concentration of raindrops with diameters this large. The relative comparisons of concentrations of large and small drop sizes will be completed later in this section when the cases will be analyzed with one another, along with a comparison with the simulated rainfall DSDs.

The rainfall event on 25 August 2005 is noticeably different to the 13 August 2005 event. This DSD plot (figure 5.1b) shows a much smaller overall drop concentration, which is indicative of much

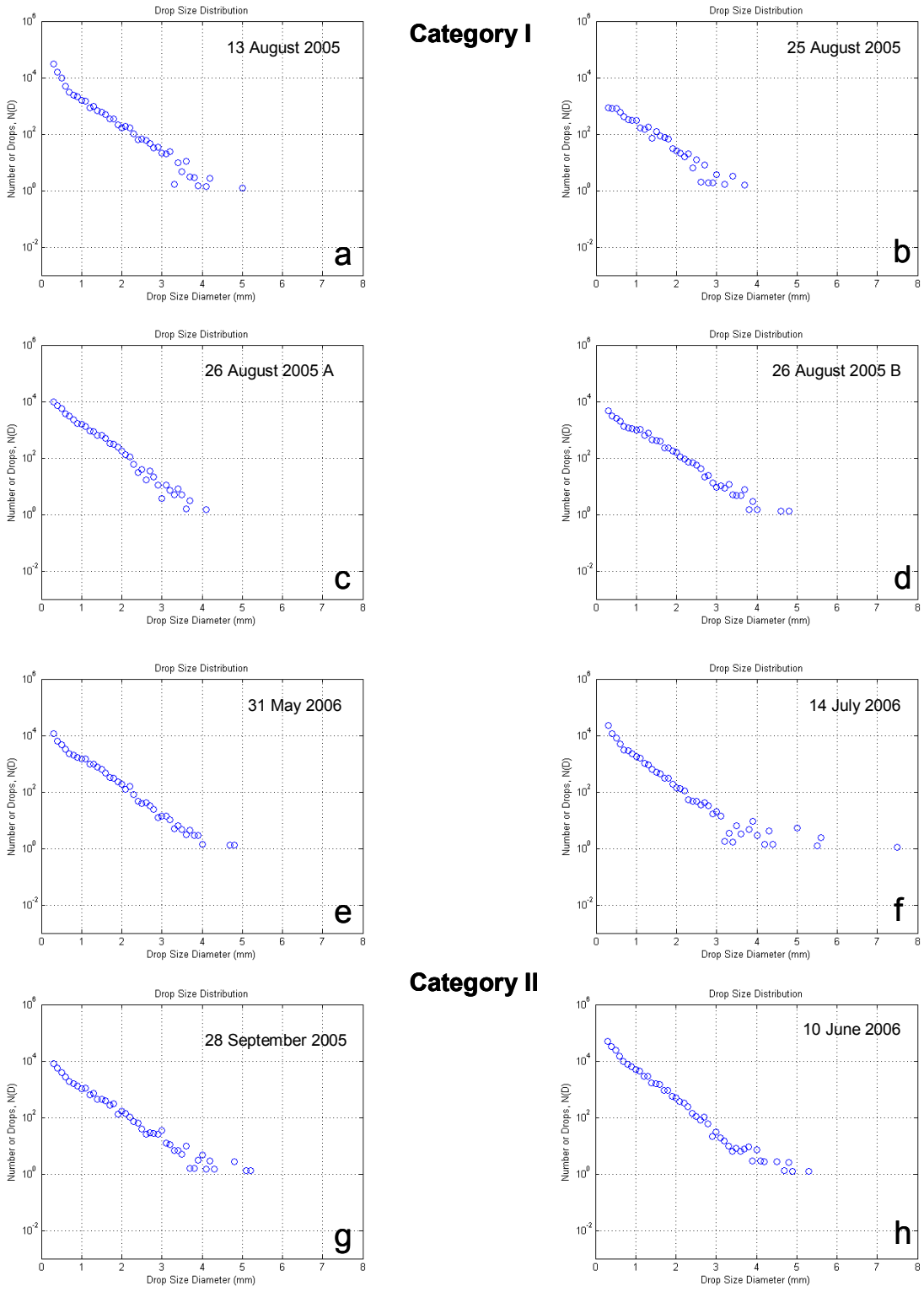

Figure 5.1: Plot of all natural DSDs throughout the study.

lower intensity rainfall. This case had the least observed R_A of 5 mm h^{-1}, lower than any other case, as shown in table 5.1. with a peak rainfall rate (R_P) of 8 mm h^{-1}. The general slope and shape of the DSD plot again resembles the LP/MP proposed distribution, with the maximum drop size diameters less than 4 mm.

Table 5.1: Data from each category I rainfall event. Data includes the peak rainfall rate (R_P), periods examined, average rainfall rate (R_A) during that period, and the total rainfall accumulation during the same period.

Date	R_P (mm h^{-1})	Period Examined (UTC)	R_A (mm h^{-1})	Period Total Rain (mm)
13-Aug-05	61	2100-2110	30	5
25-Aug-05	8	1140-1150	5	1
26-Aug-05 A	61	1226-1236	30	6
26-Aug-05 B	38	1436-1446	21	4
31-May-06	53	2330-2340	27	5
14-Jul-06	61	0312-0322	39	7

Two separate data sets were collected on 26 August 2005. The first one (case A) occurred between 1226-1236 UTC, and contained more intense rainfall than case B which occurred between 1436-1446 UTC with a R_A of 30 mm h^{-1} compared to 21 mm h^{-1}. The case A DSD plot (figure 5.1c) shows a similar shape to the previous cases, with the maximum raindrop diameter just over 4 mm. The DSD plots are similar, but the case B DSD has a smaller overall drop concentration than case A. This supports the less intense rainfall rates, even though

case B has larger maximum raindrop diameter closer to 5 mm.

The next recorded event occurred on the evening of 31 May 2006. The period examined was from 2330-2340 UTC, containing a R_A of 27 mm h^{-1}. As in the other natural cases, this event had a similar DSD curve characteristic to an exponential distribution, supporting the LP/MP proposed technique for low intensity rainfall (figure 5.1e). Maximum raindrop diameters approached 5 mm.

The final category I rainfall event occurred on 14 July 2006 from 0312-0322 UTC. The maximum observed raindrop diameters exceeded 7 mm, much higher than any other natural rainfall event captured in this study. At a first glance this DSD plot (figure 5.1f), one would expect the rainfall intensity to be greater than the other cases due to the greater concentration of raindrops with large diameters. The observed R_A (table 5.1) was 39 mm h^{-1}, with R_P of 61 mm h^{-1}. At this time, it is possible that the graphical inconsistency could be explained by very small, wet hail, or some other unforeseen factor. However, no hail was actually observed on-site or reported nearby.

All category I rainfall events had DSD plots that resembled the exponential distribution. This is consistent with the low intensity rainfall rates that have been believed to produce the exponential DSD plots, with all storms recording rainfall rates of 40 mm h^{-1} or less. The category II events had rainfall rates greater than those in category I

rainfall events. Table 5.2 shows the data for both cases, with peak rainfall intensities as great as 152 mm hr^{-1}. As described in Chapter 4, these events were of the convective, high-energy nature, and may not be accurately represented by the exponential distribution proposed by LP/MP. Recent research has indicated that the convective, high-energy rainstorms are best represented by a statistical gamma distribution (Testud *et al*. 2001). From this, one would expect DSDs of the category II events to follow the gamma distribution.

Table 5.2: Data from category II events. Data includes the peak rainfall rate (R_P), periods examined, average rainfall rate (R_A) during that period, and the total rainfall accumulation during the same period.

Date	R_P (mm h^{-1})	Period Examined (UTC)	R_A (mm h^{-1})	Period Total Rain (mm)
28-Sep-05	99	1706-1716	43	8
10-Jun-06	152	2314-2324	114	23

The first category II case occurred from 1706-1716 UTC on 28 September 2005. Note that the shape of the DSD plot is very similar to all other natural rainfall cases presented here, likely represented by an exponential curve (figure 5.1g). This 28 September 2005 case had a R_A of 43 mm h^{-1}, with total rainfall accumulation of 8 mm throughout the 10-minute period. Looking at those statistics, the comparison with the category I events shows those cases had similar results. Drop

diameters did exceed 5 mm. The similarities with category I events in regard to rainfall intensity and rainfall accumulation might explain the exponential DSD characteristics.

The final event analyzed in this study occurred on 10 June 2006, from 2314-2324 UTC. This case recorded the most intense R_A and R_P, at 114 and 152 mm h^{-1}, respectively (table 5.2). Over the 10-minute time period examined, 23 mm of rainfall accumulated. It should be noted that, while 23 mm of rainfall was observed, the R_A was 114 mm h^{-1}, not the 138 mm h^{-1} the math may suggest. This presents the limitation of the tipping bucket rain gauge used in this study, where rainfall intensities over 51 mm h^{-1} tend to be underestimated. Figure 5.1h shows this DSD plot from the observed data, which has similar curve characteristics to all other cases presented. Maximum rain drop diameters did exceed 5 mm, but other cases in this study had much larger drop sizes. Even with the extreme rainfall intensity recorded with this data set, the DSD plot still resembles an exponential curve. This case shows little difference with the other cases, and does not support the assumption that high-intensity, convective-type rainfall is more accurately represented by a gamma distribution as proposed in recent research (Testud *et al*. 2001). The numerical analysis will delve into detail the comparison of the results presented here to those from Testud *et al.* (2001).

Overall, the graphical analyses completed here show that the natural rainfall DSDs have characteristics that are similar to the exponential distribution curve proposed by LP/MP. The results from the greatest intensity rainfall case show a better correlation with the exponential curve than the gamma DSD fit curve proposed by recent studies (Testud *et al*. 2001). The graphical analysis here shows the DSD plots that have greater overall drop concentrations with relatively large numbers of small and large diameter raindrop are those cases where the rainfall rates are greatest. When the overall drop concentration is less, with smaller numbers of large raindrops, the rainfall intensity is generally less. More research is required for sufficient scientific evidence to support the theory that natural rainfall as a result of high-energy, convective-type storms is best characterized by a statistical gamma DSD rather than the exponential form of the gamma DSD.

5.1.2 Simulated Rainfall

Since one hypothesis of this study involves comparing natural rainfall DSDs to those DSDs generated from simulated rainfall, data were collected using the same RIS as the field data collection. Figure 5.2 shows the DSD plots gathered from data on 28 July 2005 with a simulated rainfall rate of 135-145 mm h^{-1} for the various distances the

screen was placed beneath the dripper tank. Varying the screen distance allows for changing the DSD characteristics produced by the simulator, while keeping a near-constant rainfall rate. As discussed in Chapter 3, when the screen distance is greater, larger concentrations of smaller raindrops should be present. When the screen is set at smaller distances, there should be a relatively greater concentration of raindrops of larger diameters. This relative concentration of drops is evident in the DSDs shown in figure 5.2. The concentration of

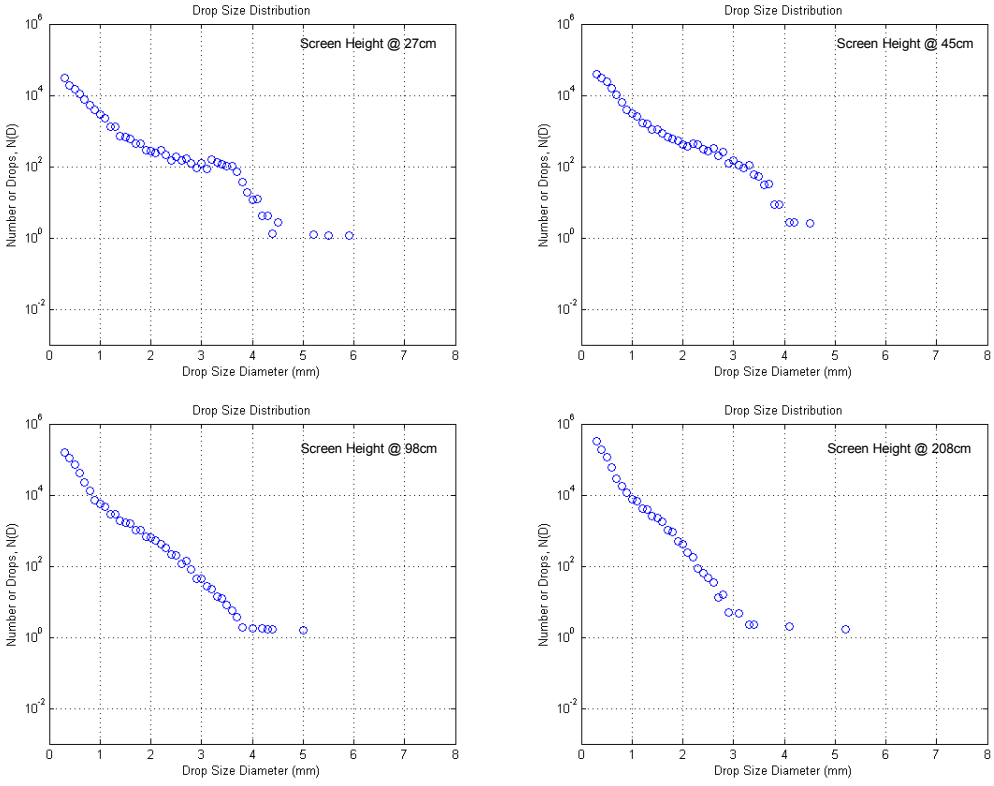

Figure 5.2: DSD plot of simulated rainfall data gathered from the indoor rainfall simulator on 28 July 2005. The screen heights below the dripper tank are located in the upper right portion of the plots.

raindrops with large diameters decreases as the screen distance increases. To compensate for the smaller concentration of larger raindrops, and keeping rainfall rate nearly constant, a large increase in the number of smaller raindrops is evident with numbers approaching 10^6 drops m^{-3} from near 10^4 drops m^{-3} when decreasing the screen distance to 208 cm from 27 cm.

Figure 5.3 shows another sample of simulated rainfall DSDs gathered on 09 November 2006. Similar to data shown in figure 5.2,

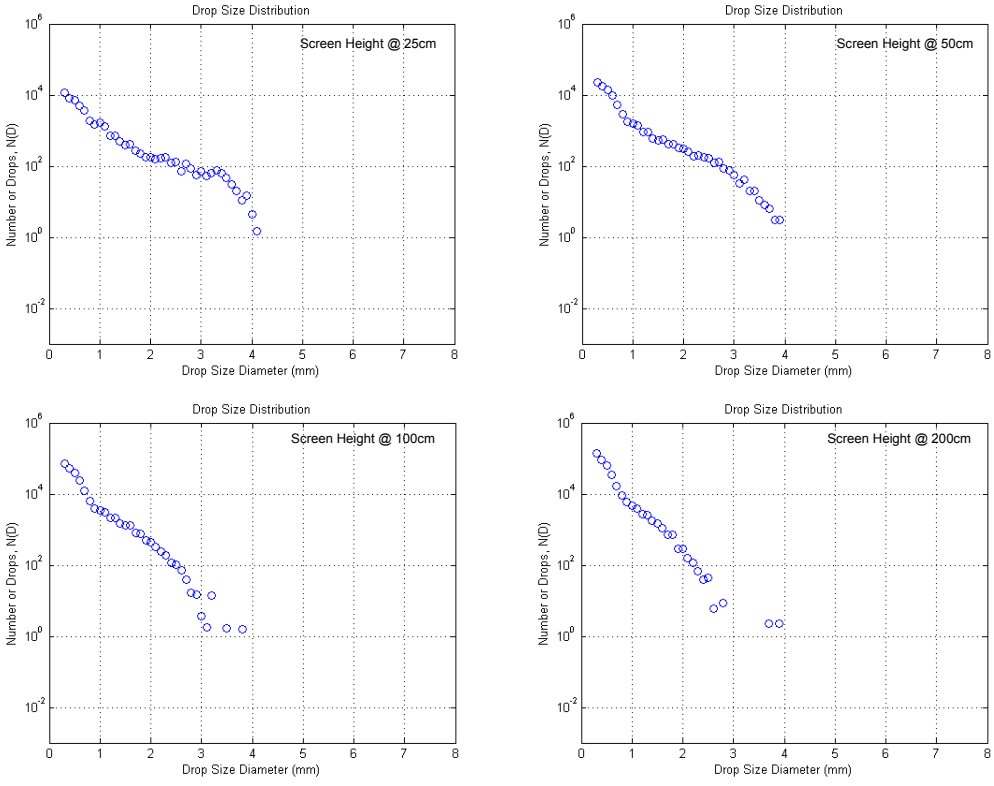

Figure 5.3: DSD plot of simulated rainfall data gathered from the indoor rainfall simulator on 09 November 2006. The screen heights below the dripper tank are located in the upper right portion of the plots.

the rainfall intensity was nearly constant from 85-105 mm h^{-1} throughout the data collection. The DSD plots generated on this day are consistent with figure 5.2 and the expected results discussed in chapter 3 on the indoor rainfall simulator. Since the rainfall rate was nearly constant, only the DSD changes as the screen distance is varied. Another aspect to note is the maximum diameter drop size never exceeds 6 mm with the simulator, and even those large drops are low in concentration.

The general shapes of the DSD plots in figures 5.2 and 5.3 are similar to those discussed in the natural rainfall events. The slopes of the curves increase and median drop size diameter decreases as screen distance increases. The concentration of large diameter raindrops increases as the redistribution screen get close to the dipper tank. These plots resemble the exponential fit curve evident in most of the natural cases, and proposed by LP/MP.

5.2 Quantitative Analysis

5.2.1 Natural Events

Figure 5.4 shows the DSD plots from the natural rainfall events with a gamma-fit curve plotted. These curves were developed using the gamma distribution equation (2.3), where N_T, μ, and Λ are computed by fitting the actual DSD plot. The total number of drops

(N_T) and Λ are the y-intercept and slope, respectively. The parameter μ is the shape of the gamma distribution curve. When μ is positive, the natural DSD will begin to mimic the gamma distribution technique proposed by Testud *et al*. (2001). When μ is near 0 (+/-), the gamma distribution curve takes on exponential distribution characteristics. Table 5.3 shows the gamma distribution parameters derived from the natural rainfall DSD plots. These parameters represent the curves fitted to the DSD data.

The gamma distribution curves plotted over the DSD data from the natural rainfall events all fit well upon visual inspection, with each gamma distribution curve shown in this study generated using a 95% confidence level. Looking at the gamma distribution data in table 5.3, a wide range of values for N_T is observed, ranging from 5.50×10^3 to 1.73×10^5 drops m^{-3}, from the lightest to the greatest observed R_A. The slopes varied from 2.55 to 2.95 mm^{-1}, with no real discernable trends with respect to rain rates. The parameter of greatest interest is μ since this study is relating natural rainfall DSDs to simulated DSDs, and comparing these DSD results to previous work where μ determines the shape of the gamma fit curve. In most of the natural rainfall events presented here, all μ values are near zero. The rainfall event on 25 August 2005 had the μ of 0.63 that is furthest from the

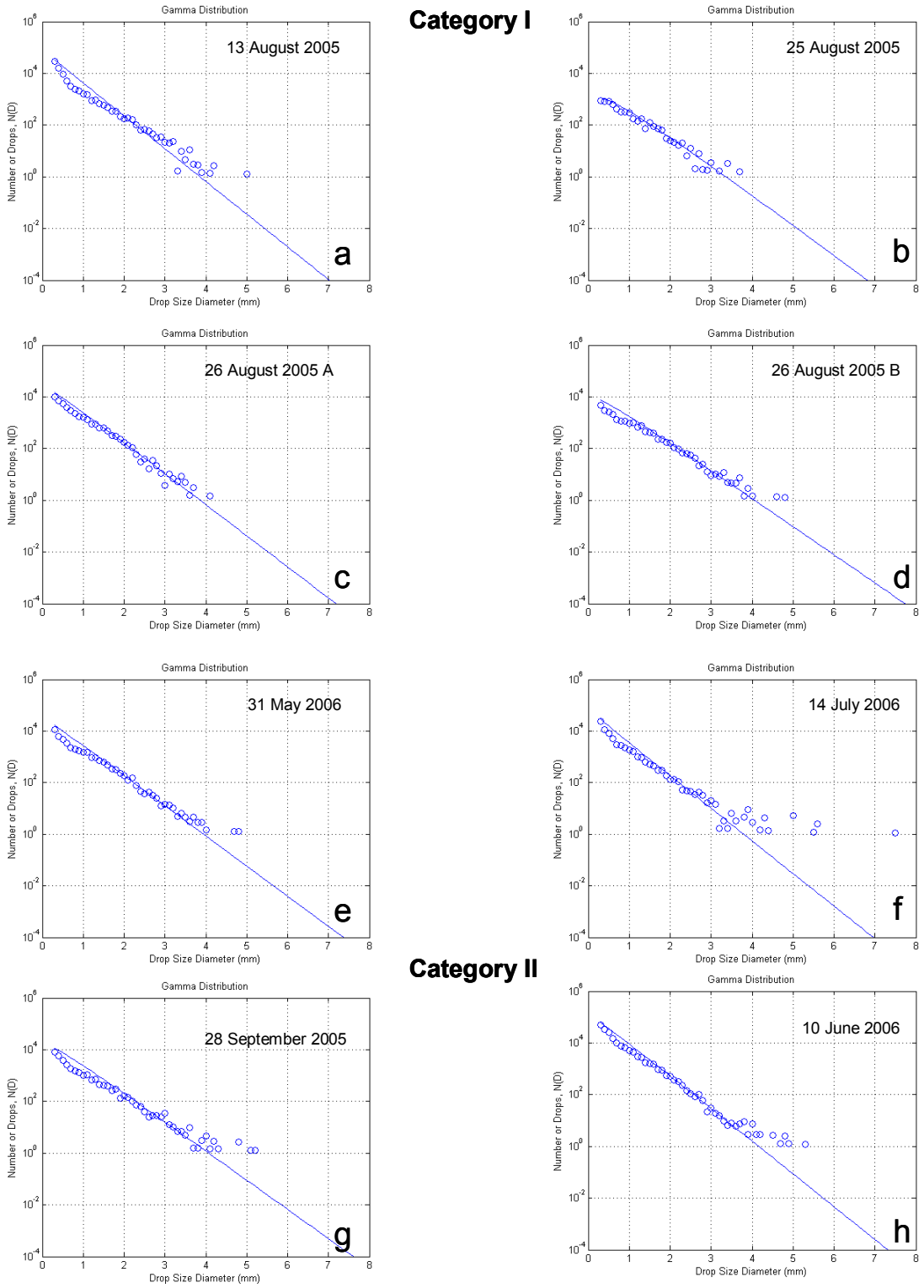

Figure 5.4: Plot of the natural DSD with gamma-fit curve superimposed.

Table 5.3: Gamma distribution parameters N_T (drops m^{-3}), μ, Λ (mm^{-1}), and corresponding D_0 (mm) for the natural rainfall events.

Date	Time Interval	N_T	μ	Λ	D_0
13-Aug-05	2100-2110	7.70E+04	-0.05	2.90	1.2
25-Aug-05	1140-1150	5.50E+03	0.62	2.79	1.5
26-Aug-05 A	1226-1236	4.00E+04	0.15	2.80	1.4
26-Aug-05 B	1436-1446	2.20E+04	0.25	2.55	1.5
14-Jul-06	0312-0322	6.40E+04	-0.05	2.90	1.2
31-May-06	2330-2340	4.00E+04	0.05	2.70	1.4
28-Sep-05	1706-1716	3.40E+04	0.25	2.65	1.5
10-Jun-06	2314-2324	1.72E+05	0.15	2.95	1.3

exponential, or closest to the gamma distribution proposed by Testud *et al*. (2001) compared to the other events here. This is interesting since this rainfall event had the lowest intensity rainfall observed in this study. The gamma distribution technique was proposed to mimic high-intensity, convective rainfall more closely than the low intensity rainfall. Upon further investigation, the near-0 values for μ may not differ significantly with the results from Testud *et al*. (2001). Table 5.4 shows the results from Testud *et al*. (2001) where 7112 drop size spectra were obtained.

When comparing μ values from the cases discussed in this study to those from Testud *et al*. (2001), the mean μ values from table 5.4 are larger, and more positive than results shown here. However, high variability in μ is evident when looking at the standard deviation of μ.

Table 5.4: Results from Testud *et al*. (2001) showing μ and standard deviation with C denoting convective rainfall of the intensity within parentheses.

Storm Type	**μ**	**std. dev**
Stratiform	0.86	1.28
C(0-10 mm h^{-1})	1.51	2.98
C(10-30 mm h^{-1})	1.78	2.36
C(30-100 mm h^{-1})	0.85	1.08

For example, one standard deviation of μ in the convective type precipitation (10-30 mm h^{-1}) is +/- 2.36, with μ ranging from -0.58 to 4.14. All values of μ in this study fall within one standard deviation of the mean μ values from Testud *et al*. (2001), showing statistically reasonable correlation between these results and those from Testud *et al*. (2001). Also, since only eight raindrop size spectra were analyzed here, more spectra samples may give additional support to the results from Testud *et al*. (2001).

It should be noted that the spectra collected in the Testud *et al*. (2001) study were gathered using the NCAR Electra aircraft from 21 flights out of Honiara, Guadalcanal, observing deep convection over the west Pacific Ocean. These measurements were taken from an altitude of 3 km, not at the surface like the spectra gathered in this study. Testud *et al*. (2001) results may not capture all characteristics of DSDs near the surface. However, there were not enough data gathered in this study to demonstrate that the near-surface DSD

characterizations are different.

Research from Illingworth and Blackman (2002) show mean μ values of 5 to 6, with a standard deviation of 5 for convective rainfall in the Tropics and Mid-Latitudes. This is more variable than results from Testud *et al*. (2001) (table 5.4) and those results here. The mean μ for this study near 0 at 0.17 with a standard deviation of 0.22, a relatively minimal variability in μ compared to either Testud *et al*. (2001) or Illingworth and Blackman (2002).

5.2.2 Simulated Rainfall

The same gamma distribution curve technique used in the numerical analysis of the natural rainfall events was used to describe the simulated rainfall. Figure 5.5 shows the gamma distribution curves plotted over the DSD data on 09 November 2006. The gamma distribution curve mimics the DSD plot fairly accurately at the 95% confidence level, with the best correlation occurring with those DSD plots where the screen height was at increasing distances below the dripper tank.

Table 5.5 lists the gamma distribution parameters from the curves in figures 5.5 and 5.6. All sample sets had similar shapes with μ near 0. The variations were associated with N_T and Λ as the drop concentration and slope of the curve both increase as the screen

distance was greater. Since the rainfall rates were kept nearly constant, the increase in overall drop concentration as the slope increased shows, numerically, how the gamma distribution-derived rainfall rates are also nearly the same with the varying screen distances. Table 5.6 shows the median drop size diameter (D_0) for the simulated rainfall. Note the decrease in D_0 as the redistribution screen distance increases. The other simulated rainfall data set showed very similar numerical results. Figure 5.6 shows the gamma distribution curves plotted over the actual DSD data for 28 July 2005, and table

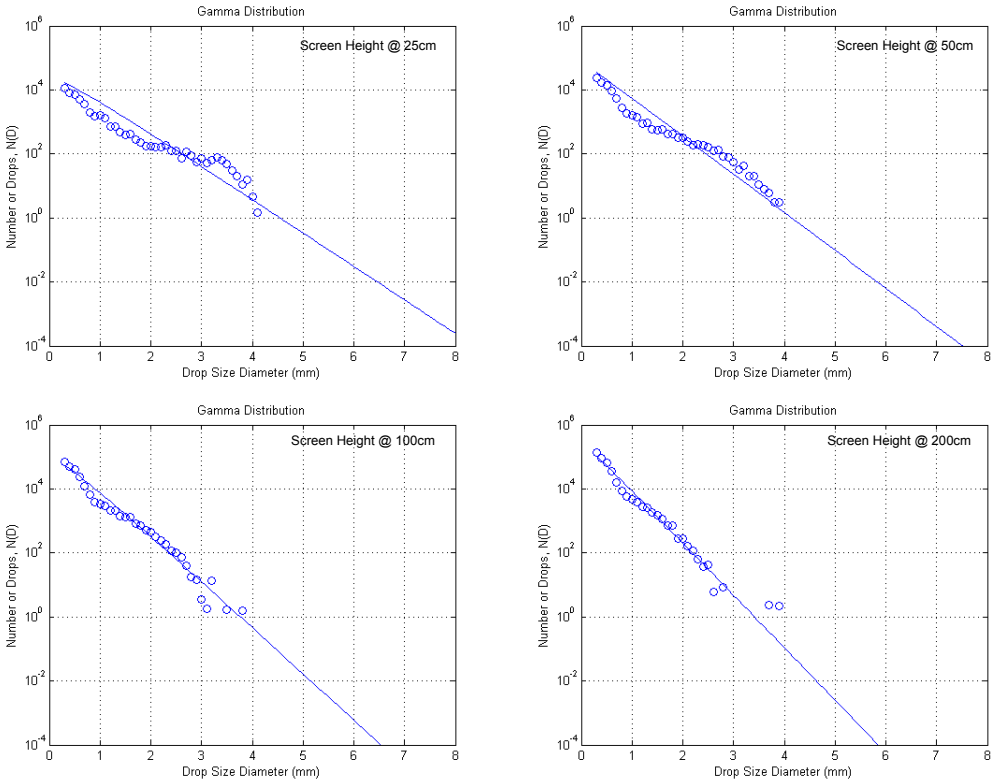

Figure 5.5: DSD plot from 09 November 2006.

5.5 shows the parameters associated with those gamma curves. The only difference between the two simulated events was the set rainfall intensity of 135-145 mm h^{-1} for the 28 July 2005 case and 85-105 mm h^{-1} for 09 November 2006, and the slight variations in screen height. One noticeable difference concerning the simulated rainfall data is the lack of large raindrop diameters. The abrupt downward slope of the DSD data at the upper range of the raindrop diameters shows one limitation of the indoor rainfall simulator.

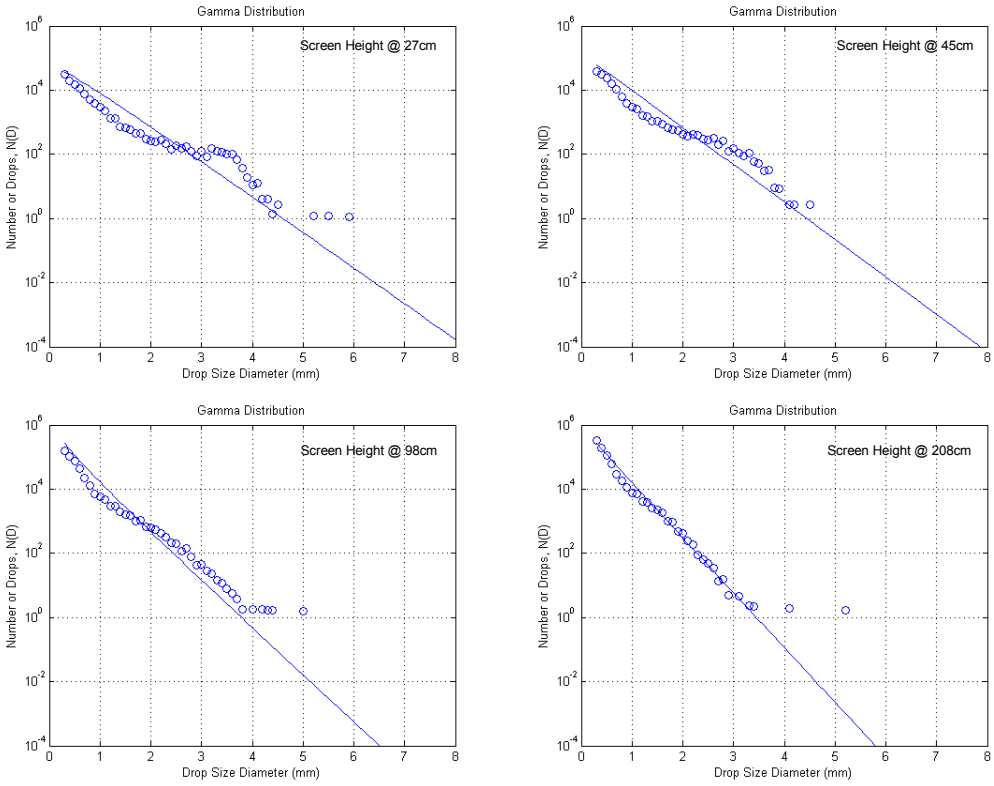

Figure 5.6: DSD plot from 28 July 2005.

Table 5.5: Gamma distribution parameters N_T (drops m^{-3}), μ, and Λ (mm^{-1}) gathered from simulated rainfall from 09 November 2006 and 28 July 2005.

	N_T	μ	Λ		N_T	μ	Λ
9-Nov-06				*28-Jul-05*			
25 cm	4.70E+04	0.25	2.45	*27 cm*	1.08E+05	0.25	2.60
50 cm	8.40E+04	0.05	2.75	*45 cm*	1.47E+05	0.05	2.70
100 cm	2.27E+05	0.35	3.40	*98 cm*	4.53E+05	-0.40	3.30
200 cm	3.81E+05	0.10	3.80	*208 cm*	7.92E+05	-0.10	3.90

Table 5.6: Median drop size diameters D_0 calculated from Λ for the data from the simulated rainfall.

9-Nov-06	**D_0 (mm)**	***28-Jul-05***	**D_0 (mm)**
25 cm	1.6	*27 cm*	1.5
50 cm	1.4	*45 cm*	1.4
100 cm	1.2	*98 cm*	1.0
200 cm	1.0	*208 cm*	0.9

5.2.3 Kinetic Energy Analysis

Before kinetic energy (KE) was calculated, a numerical calculation of the rainfall intensities from the DSD data (R_S) and gamma distribution parameters (R_G) was completed. R_S is the rainfall rate derived from the summation of raindrop diameters, while R_G was calculated from the gamma distribution curves shown in section 5.2.2 using equation 2.17. Table 5.7 shows those rainfall rates for the natural events. The analysis shows that both R_S and R_G tend to over-estimate the rainfall intensity when compared to the observed R_A, except for the category II events. All category I events had lower R_A

than R_S and R_G.

The category II events seem to have a better correlation between the R_A and the R_S and R_G. The calculated rainfall intensities were similar to those observed R_A. No definite conclusion can be made from the differences in observed and calculated rainfall intensities without more data from rainfall events with very heavy rainfall similar to the 10 June 2006 case.

Table 5.7: Comparison of observed rainfall intensity (R_A in mm h^{-1}) to numerical calculations for rainfall rate by drop diameter summation (R_S), gamma distribution parameters (R_G), drop diameter summation kinetic energy (KE in W m^{-2}) and total kinetic energy flux (KE_T), observed wind speed (u in m s^{-1}), and gamma distribution derived kinetic energy (KE_T) and total kinetic energy flux (KE_{TG}).

Date	Period Examined	R_A	R_S	R_G	KE	KE_G	u	KE_T	KE_{TG}
13-Aug-05	2100-2110	30	49	55	0.62	0.43	7.9	1.48	1.97
25-Aug-05	1140-1150	5	7	6	0.09	0.06	0.8	0.09	0.06
26-Aug-05 A	1226-1236	30	37	37	0.47	0.31	0.9	0.48	0.32
26-Aug-05 B	1436-1446	21	33	33	0.42	0.33	1.0	0.43	0.34
31-May-06	2330-2340	27	41	42	0.53	0.36	2.1	0.58	0.43
14-Jul-06	0312-0322	39	45	46	0.57	0.35	6.4	1.08	1.03
28-Sep-05	1706-1716	43	37	43	0.48	0.40	1.7	0.51	0.45
10-Jun-06	2314-2324	114	116	111	1.47	0.81	6.8	2.96	2.64

Since the calculated rainfall rates seem to over-estimate the observed rainfall rates, the kinetic energy values may be expected to be over-estimated for some of the natural events. Even with this issue, the kinetic energies were calculated using equations 2.16 and 2.19.

The kinetic energy flux from summation of raindrop diameters (KE) was calculated using the theoretical terminal velocity from Ulbrich (1983), and KE_G from the gamma distribution parameters. Table 5.7 contains these values for the natural rainfall events.

The first thing to note is the variation of KE and KE_G with a change in the R_S and R_G. For instance, when the R_S was 7 mm h^{-1}, the KE was 0.09 W m^{-2} compared to a more intense R_S at 41 mm h^{-1} with KE of 0.53 W m^{-2}. For 10 June 2006, the KE was 1.97 W m^{-2} with the highest R_S. This change occurs because the formulations of KE and KE_G use calculated values of R_S and R_G, not the actual R_A. While using the observed R_A to calculate kinetic energy flux would seem more accurate in calculating kinetic energy, this study requires the use of the derived quantities to get values for kinetic energy in comparison to the observed R_A. This will allow future studies to come up with better estimations of kinetic energy based on those observed rainfall rates and rainfall accumulations. Another aspect to note is the differences between KE and KE_G. In all natural rainfall events, KE_G was lower than KE, and with less variability in changes of rainfall intensity than KE. For this thesis, relating KE and KE_G is for comparison purposes only, and more emphasis was given to the KE_G since the majority of the background was based on analysis techniques using a gamma distribution. However, any significant outcomes from the relationship

between raindrop diameter summation and the gamma distribution parameters will be noted for future work.

Since some of the basis of this study involved relating current soil loss calculations on the Marshall and Palmer (1948) DSD, the kinetic energy calculation used in the RUSLE was calculated for comparison to KE and KE_G. The relationship for the kinetic energy from the RUSLE (Schwab *et al*. 1993), KE_R, is calculated from R_A, and total rainfall accumulation for the time of interest, R_T, and is shown by

$$KE_R = \frac{\left[0.119 + \left(0.0873 \log R_A\right) R_T\right]}{6} \tag{5.1}$$

The KE_R is shown in table 5.8, along with the KE and KE_G. The kinetic energy flux calculation was overall lower in magnitude than KE and KE_G, except for the 10 June 2006 event. KE_R tends to under-estimate the energy flux for the lower intensity storms, but fell between KE and KE_G for the most intense rainfall event. The explanation for this can be described by the use of observed R_A and total period rainfall accumulation used in the calculation. Since KE and KE_G tend to over estimate the rainfall intensity, KE_R uses the information that was actually observed. However, this assumption is bases on assumed DSDs from Marshall and Palmer (1948). The results from this study show DSDs more similar to those DSDs proposed by Marshall and Palmer (1948), or where μ is zero.

Table 5.8: Comparison of kinetic energy flux KE_R from the RUSLE formulation (equation (5.1)) to KE and KE_G (all W m^{-2}).

Date	**KE**	**KE_G**	**KE_R**
Category I			
13 August 2005	0.62	0.43	0.21
25 August 2005	0.09	0.06	0.03
26 August 2005 A	0.47	0.31	0.25
26 August 2005 B	0.42	0.33	0.16
31 May 2006	0.53	0.36	0.20
14 July 2006	0.57	0.35	0.30
Category II			
28 September 2005	0.48	0.40	0.35
10 June 2006	1.47	0.81	1.14

The data for the horizontal contribution to the overall kinetic energy data in is also shown in table 5.7. Total kinetic energy from drop diameter summation (KE_T) and gamma distribution parameters (KE_{TG}) were calculated using the 10-minute mean horizontal observed wind (u in m s^{-1}) averaged from heights 0.75 and 1.5 m AGL, using equation 2.19. As one would expect, more kinetic energy flux is estimated when u is greater. It may also be expected that the rainfall event with the strongest u to have the greatest horizontal wind contribution. Looking at table 5.7, this is indeed the case, where the rainfall event on 13 August 2005 had the horizontal wind influence due

to the strongest *u* at 7.9 m s^{-1}. However, since this rainfall event contained moderate rainfall rates, the overall total kinetic energy fluxes were not the greatest with KE_T and KE_{TG} of 1.48 and 1.97 W m^{-2}, respectively. The rainfall event with the greatest KE_T and KE_{TG} was the 10 June 2006 case. Not only did the heaviest rainfall occur on this date, but the second strongest wind of 6.8 m s^{-1} occurred as well. It was the combination of both horizontal influence and heavy rainfall that contributed to the large KE_T and KE_{TG} of 2.96 and 2.64 W m^{-2}, respectively.

In the cases where rainfall rates and *u* were less intense, horizontal winds have small contributions to the total kinetic energy flux. On 25 August 2005, there were both light rain and weak *u* at 0.8 m s^{-1}. The KE_T and KE_{TG} had no increase over the KE and KE_G of 0.09 and 0.06 W m^{-2}, respectively, which use just the theoretical terminal velocity as the sole component. The other case to mention took place the following day with greater rainfall intensity for both case A and B. Since *u* was 0.9 and 1.0 m s^{-1}, respectively, very little contribution was made to the KE_T and KE_{TG}. For this case, it should be noted that both cases had a slight increase of 0.01 W m^{-2}, even though case A had a greater rainfall rate than B. What makes up for greater rainfall intensity is the slightly weaker *u*.

As stated in Chapter 2, Helming (2001) concluded that horizontal wind effects account for approximately one-fourth of the total kinetic energy in rain storms. The next step in analyzing the horizontal contribution from the natural rainfall events was to see if our results come to a similar conclusion to Helming (2001). While some of the extreme rainfall events had horizontal kinetic energy flux from drop diameter summation (KE_H) and gamma distribution parameters (KE_{HG}) that accounted for more than 50% of the KE_T and KE_{TG}, the other, less intense storms have very little additional contributions. Table 5.9 shows the values for KE_H and KE_{HG}, and what percentages of KE_T and KE_{TG} that KE_H and KE_{HG} represent. When the average of all horizontal contributions to kinetic energy for the entire study are calculated, the percentage that KE_H and KE_{HG} represent was 39% and 58%, respectively, a larger contribution than the conclusion from Helming (2001).

Realizing that averaging KE_H and KE_{HG} for the entire study does not truly represent all cases presented here (since rainfall events either had much less contributions or much greater contributions than the mean), categorizing the contributions into different classifications of wind speed my be a better representation. The average horizontal contribution of total kinetic energy was calculated for rainfall events with u less than and greater than 5.0 m s^{-1}. This resulted in KE_H and

KE_{HG} accounting for 5% and 9%, respectively, of the KE_T and KE_{TG} for the five rainfall events with *u* of less than 5.0 m s^{-1}. The contribution from KE_H and KE_{HG} were much greater at 52% and 72%, respectively, for the three rainfall events with *u* over 5.0 m s^{-1}. This result shows that more than half of the energy contained within the most intense (by wind and turbulence) rainfall events is estimated from horizontal wind influences. Less than 10% of the total kinetic energy is estimated from horizontal wind influence in storm with relatively weak *u* values. This shows that wind velocity may greatly influence the total kinetic energy contained within some rainstorms.

It should be noted that the storm characteristics experienced during the Helming (2001) study included a study mean *u* of 3.2 m s^{-1}, R_A of 1.8 mm h^{-1}, and a R_P of 83.4 mm h^{-1} over 180 rainfall events, (statistically a more desirable sample size over this study's 8 events). The results presented here represent a study mean *u* of 3.5 m s^{-1}, similar to those presented by Helming (2001). However, the data from this study had a R_A of 39 mm h^{-1}, with a R_P of 152 mm h^{-1}. While the study mean *u* were similar, this study contained much greater and a wider range of rainfall intensities, evidence of the different climates associated with the Central United States compared to Müncheberg, Germany. These reasons could explain why the horizontal contribution did account for almost one-half the total kinetic energy flux,

significantly more than the Helming (2001) conclusion.

The next analysis looks at the kinetic energy flux derived from DSD data from the indoor rainfall simulator, since the basis of this study was to compare the kinetic energy flux of natural rainfall DSD to DSDs of simulated rainfall. It should be first noted that the indoor rainfall simulator cannot replicate the horizontal wind environment found in observed natural rainfall. Therefore, the total kinetic energy flux is identical to kinetic energy flux from vertically falling, simulated rainfall. This immediately exposes one of the limitations associated with an indoor rainfall simulator. In many instances, natural rainfall events include variable wind velocities throughout the duration of the event. In many cases, the turbulence associated with the greatest energy rainstorms would be extremely difficult to replicate in a laboratory environment, or in numerical calculations. In any case, it is still reasonable to compare natural to simulated rainfall, so one can get a sense of what adjustments can be made to account for such variations while mimicking rainfall.

Table 5.10 shows the kinetic energy flux for the different screen heights for both days' where data were collected with the simulator. The main aspect to notice is the decrease in KE_G as screen distance increases. Even though rainfall intensity is nearly constant for each respective date, the KE_G can be altered by varying screen distance

below the dripper tank, thus altering the DSD of the raindrops produced by the simulator. Also, KE_G increases as a function of rainfall rate, which is shown in table 5.10 since the data gathered on 09 November 2006 had a lower intensity rainfall than the 28 July 2005 case. Altering the rainfall rate and varying the screen distance provided the best possibility for the rainfall simulator to mimic natural

Table 5.9: Comparison of KE_T and KE_{TG} to horizontal kinetic energy flux calculated from drop volume and gamma distribution parameters (KE_H and KE_{GH}, respectively), and the percentage of KE_T and KE_{TG} that KE_H and KE_{HG} represents (all in W m^{-2}).

Date	Period Examined	KE	KE_G	KE_T	KE_{TG}	KE_H	KE_{HG}	$\%KE_T$	$\%KE_{TG}$
13-Aug-05	2100-2110	0.62	0.43	1.48	1.97	0.86	1.54	58%	78%
25-Aug-05	1140-1150	0.09	0.06	0.09	0.06	0.00	0.00	0%	0%
26-Aug-05 A	1226-1236	0.47	0.31	0.48	0.32	0.01	0.01	2%	3%
26-Aug-05 B	1436-1446	0.42	0.33	0.43	0.34	0.01	0.01	2%	3%
31-May-06	2330-2340	0.53	0.36	0.58	0.43	0.05	0.07	9%	16%
14-Jul-06	0312-0322	0.57	0.35	1.08	1.03	0.51	0.68	47%	66%
Category II						**Mean**		**35%**	**56%**
28-Sep-05	1706-1716	0.48	0.40	0.51	0.45	0.03	0.05	6%	11%
10-Jun-06	2314-2324	1.47	0.81	2.96	2.64	1.49	1.83	50%	69%
						Mean		**44%**	**61%**
					Study Mean			***39%***	***58%***

rain. Again, the biggest discrepancy deals with trying to incorporate the influence of horizontal wind when estimating kinetic energy flux.

When comparing natural and simulated rainfall directly using KE_G, few similarities exist. This is most likely due to differences in the rainfall rates set with the simulator at the time of data collection and the rainfall intensity of the natural events. The lowest rainfall intensity used was around 85 mm h^{-1}. Only one rainfall event recorded during this study contained heavy enough rainfall to be compared with the results from the rainfall simulator. That rainfall event occurred on 10 June 2006, with R_A of 114 mm h^{-1}. Looking at the 09 November simulated case, the screen height set at the shortest distance of 25 cm produced KE_G of 0.91 W m^{-2}, with a rainfall rate of approximately 80

Table 5.10: Comparison of calculated rainfall rates R_S and R_G (mm h^{-1}), and kinetic energy flux (W m^{-2}) from both drop volume and gamma distribution parameters (KE and KE_G, respectively) for the simulated rainfall data sets from 09 November 2006 and 28 July 2005.

	R_S	R_G	KE	KE_G		R_S	R_G	KE	KE_G
9-Nov-06					*28-Jul-05*				
25 cm	74	87	0.95	0.91	*27 cm*	140	149	1.78	1.44
50 cm	74	80	0.94	0.68	*45 cm*	152	153	1.93	1.33
100 cm	89	86	1.14	0.60	*98 cm*	150	168	1.76	0.98
200 cm	85	80	1.08	0.45	*208 cm*	140	144	1.78	0.74

mm h^{-1}. The KE_G for 10 June 2006 was 0.81 W m^{-2}, about 0.10 W m^{-2}, less than the simulated case. Looking at the 28 July simulated case, the screen height set at the largest distance of 208 cm produced KE_G of 0.74 W m^{-2}, but with a much higher rainfall rate of about 140 mm h^{-1}. It is suggested that further analysis be completed with the simulator at multiple rainfall rates, while also varying screen distance at a finer resolution than those chosen in this study. This would require adjusting the drop redistribution screen at either 5 or 10 cm intervals between 25 and 200 cm. Keeping the rainfall rate constant during the 10 to 15 minute sampling interval at each screen height would require at least 3 hours time. This time required does not include the time needed for preparing the simulator and adjusting the screen height which requires substantial additional time. This experiment alone can take considerable time just for one rainfall intensity, and adjusting the rainfall rate can further lengthen the time dedication. The possible results from this proposed study can be compared to the results shown here and the results from more natural cases using the same equipment. It is hypothesized that matching the rainfall rate of a natural rainfall event with the rainfall simulator, and then varying screen height will produce best results in mimicking natural rainfall, neglecting horizontal wind.

5.3 Soil Erosion

Quantifying soil loss in natural rainfall events and comparing those results to known soil loss data from simulated rainfall was another goal of this study. However, complications in observing soil runoff and ponding, along with safety concerns associated with observing ponding times made this aspect of the study difficult, and resulted in limited data. While more data are required for reasonable scientific results, a discussion of what data were gathered, and issues regarding the lack of data will be presented.

After redesigning the soil beds used in the field study during the summer of 2005, one natural rainfall event did produce water ponding and runoff. Unfortunately, only one soil bed was prepared for use with this case. Ideally, all three would have been ready, but the other two soil beds had already been used. The 28 September 2005 rainfall event had water ponding evident 14 minutes after rain began to fall. Figure 5.7 shows the rainfall intensity throughout the storm. Ponding was evident after the peak rainfall rate, with runoff occurring shortly after at 1716 UTC. Table 5.11 shows observed ponding times gathered from the rainfall simulator at three different rainfall intensities. The R_A used with the simulator that was closest to the observed R_A on this day was 64 mm h^{-1}. Approximately 8-9 minutes passed before ponding was evident with the simulator, while it took 14 minutes for ponding to

occur in the natural case. The longer time required for ponding can be attributed to the lower R_A, non-constant rainfall rate associated with the natural rainfall, and turbulence that is thought to limit the accumulation of rain on the soil bed used in this study. In the simulator, the rainfall rate was constant, and no winds were present.

The other natural rainfall event where runoff and ponding was evident occurred on 10 June 2006. However, in this case, the timing of surface ponding and runoff was not recorded since the thunderstorm producing the rainfall was too severe for researchers to safely observe the event. Large hail the size of quarters (26 mm diameter), winds exceeding 25 m s^{-1}, and dangerous lightning that persistently struck nearby power lines and trees provided a less-than-ideal situation for observing the actual runoff times. Only when the severity of the storm diminished was it evident that pooling and runoff had taken place. However, only 2 out of 3 soil beds showed signs of soil loss and/or ponding.

Table 5.11: Data from the indoor rainfall simulator showing times (in minutes) that water ponding occurred after rainfall was initiated. Three tests were completed at different rainfall intensities.

Intensity	128 mm h^{-1}	96 mm h^{-1}	64 mm h^{-1}
Rep 1	3.4	4.7	9.0
Rep 2	3.2	4.2	8.2
Rep 3	3.1	4.8	8.3
Mean	3.2	4.6	8.5

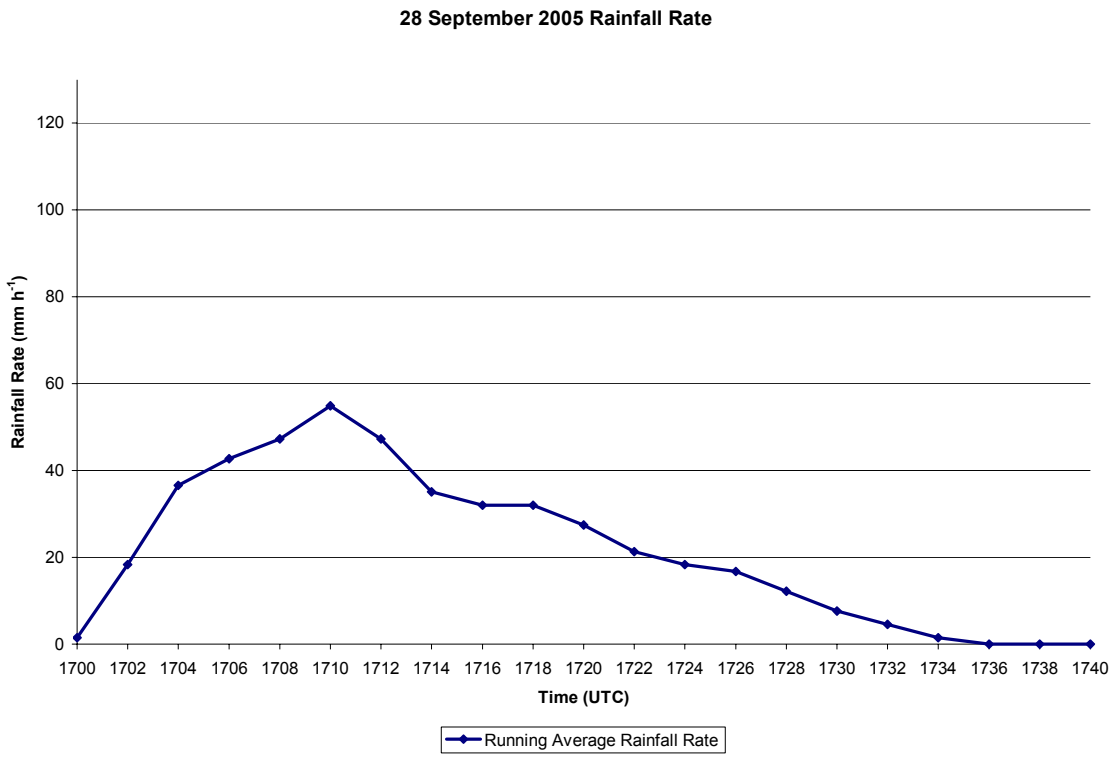

Figure 5.7: Running mean rainfall intensity for 28 September 2005 rainfall event.

This brought up questions of the significance of the orientation of the soil beds. The three soil beds were placed in three different orientations, facing northeast, southeast and northwest. It was the soil bed facing northwest that showed no signs of water pooling or runoff, with the mean wind direction from the northwest. It is thought that the design of the soil beds may interact with the overall wind velocity in preventing soil loss using this controlled experiment. Also, splash-out caused by the impact of the raindrops on the soil beds can account for some of the lack of observed soil runoff since the soil was actually lost

from being carried away from the controlled environment by the wind in the strongest storms. While six more soil beds were made to test this hypothesis, the beds were not ready in time to be used since the RIS was shipped back to the University of North Dakota, and the lack of sufficient rainfall events at the appropriate time. However, more research to test this hypothesis with multiple soil beds may provide better results when attempting to gather soil loss data using these types of soil beds in natural events. At this time, there can be no conclusive results gathered from the soil erosion portion of the study due to the lack of data.

5.4 Summary

It was hypothesized that simulated rainfall has the same characteristics as natural rainfall for drop kinetic energy as a function of rainfall intensity. This study revealed that simulated rainfall did show potential for replicating natural rainfall. The best results occurred when R_A used in the simulator was similar to the R_A of the natural rainfall event. By adjusting the redistribution screen height beneath the dripper tank, similar DSDs for natural and simulated rainfall are possible. However, there are notable issues with the simulated rainfall that one should be aware of. Those issues include limitations on maximum drop size diameter, absence of turbulence, and the lack of

rainfall rate variability using the simulator. All these factors are present in natural rainfall, and are incapable of being replicated with the rainfall simulator used in this study.

There were two different DSD curves discussed within this thesis. The curves used to represent the rainfall DSDs numerically, were a gamma curve (Testud *et al*. 2001) and a special gamma curve with the shape factor, μ, equal to zero (exponential curve) (LP/MP). The gamma curve is believed to best represent high energy, convective rainfall, while the exponential curve has historically been assumed to best represent non-convective, less intense rainfall. The hypothesis tested was that natural rainfall DSD is best represented by a gamma curve, with μ equaling zero, or an exponential curve.

This study revealed that the DSDs resemble an exponential curve with μ values near zero, from data presented here. However, these results also fall within one standard deviation of results from Testud *et al*. (2001), where results showed that a gamma distribution curve best represented convective rainfall. Analysis of more raindrop spectra may be required to see if the Testud *et al*. (2001) results can be replicated using the equipment and analysis techniques used in this study.

Since little interest has been presented with regards to the effect of horizontal wind on the kinetic energy of raindrops as they impact a soil surface, this thesis attempted to estimate the contribution of wind

in the total kinetic energy of rainfall. This estimation was based on research that showed that wind can contribute up to approximately one-fourth of the total kinetic energy contained within some rainstorms (Helming 2001). Intuitively, those storms with greater observed wind velocities will have a higher contribution of total kinetic energy from horizontal wind influences. This thesis tested whether results from Helming (2001) are representative of rainfall in the central United States. The estimation of kinetic energy from horizontal wind influence accounted for about one-half of the total kinetic energy from rainfall events analyzed in this study, a greater contribution than results from Helming (2001). This is likely because the convective storm rainfall events observed having stronger winds than rainfall events observed in the Helming (2001) study. Those rainfall events with the most intense rainfall accompanied by the strongest winds near the surface had the highest total kinetic energy, with more than one-half of the total kinetic energy contributed by horizontal motion of the drops.

The final aspect of this thesis dealt with soil erosion. The results from the hypothesis that simulated rainfall produces the same soil loss, ponding, and runoff as natural rainfall for events of equal rainfall intensity, remain inconclusive. This is due to the lack of data gathered from the field studies. Many reasons may explain the lack of data,

ranging from either the high variability of rainfall rates, near-surface turbulence preventing soil ponding, soil bed designs, and the orientation of soil beds. Simulated rainfall may overestimate the soil loss potential due to the lack of rainfall rate variability and simulation of turbulence. However, there may be an underestimation of soil loss potential from the lack of horizontal wind within the simulator. At this time, no conclusions can be made from this study other than presenting ideas for future research, covered in the following section, to possibly limit the complications this study encountered.

Chapter 6

Conclusions

6.1 Summary

Research regarding soil loss and prevention techniques has been a significant topic world wide. Soil loss is generated from both water runoff and from displacement of soil upon rain drop impact with the soil. The soil loss generated by raindrop kinetic energy flux was discussed in this thesis, specifically energy flux derived from the DSD characteristics of both natural and simulated rainfall of varying intensities. The observation of water ponding, soil displacement, and soil-water runoff timing data was attempted to compare to current soil loss research and models, and to relate DSDs and rainfall intensities to observed soil loss.

Several rainfall events were analyzed to research the DSD characteristics of natural and simulated rain. This was done to see how well simulated rainfall can replicate natural rainfall, under controlled conditions. It was hypothesized that simulated rainfall has the same characteristics as natural rainfall for drop kinetic energy as a function of rainfall intensity. This study revealed that simulated rainfall did show potential for replicating natural rainfall. The best results occurred when R_A used in the simulator was similar to the R_A of the natural

rainfall event. By adjusting the redistribution screen height beneath the dripper tank, similar DSDs for natural and simulated rainfall are possible. However, there are notable issues with the simulated rainfall that one should be aware of. Those issues include limitations on maximum drop size diameter, absence of turbulence, and the lack of rainfall rate variability using the simulator. All these factors are present in natural rainfall, and are incapable of being replicated with the rainfall simulator used in this study.

There were two different DSD curves discussed within this thesis. The curves used to represent the rainfall DSDs numerically, were a gamma curve and a special gamma curve with the shape factor, μ, equal to zero (exponential curve). The gamma curve is believed to best represent high energy, convective rainfall, while the exponential curve has historically been assumed to best represent non-convective, less intense rainfall. The hypothesis tested was that natural rainfall DSD is best represented by a gamma curve with μ equaling zero, or an exponential curve.

This study revealed that the DSDs resemble an exponential curve, with μ values near zero from data presented here. However, these results also fall within one standard deviation of results from Testud *et al*. (2001), where results showed that a gamma distribution curve best represented convective rainfall. Analysis of more raindrop spectra may

be required to see if the Testud *et al*. (2001) results can be replicated using the equipment and analysis techniques used in this study.

Since little interest has been presented with regards to the effect of horizontal wind on the kinetic energy of raindrops as they impact a soil surface, this thesis attempted to estimate the contribution of wind in the total kinetic energy of rainfall. This estimation was based on research that showed that wind can contribute up to approximately one-fourth of the total kinetic energy contained within some rainstorms (Helming 2001). Intuitively, those storms with greater observed wind velocities will have a higher contribution of total kinetic energy from horizontal wind influences. This thesis tested whether results from Helming (2001) are representative of rainfall in the central United States. The estimation of kinetic energy from horizontal wind influence accounted for about one-half of the total kinetic energy from rainfall events analyzed in this study, a greater contribution than results from Helming (2001). This is likely because the convective storm rainfall events observed having stronger winds than observed in the Helming (2001) study. Those rainfall events with the most intense rainfall accompanied by the strongest winds near the surface had the highest total kinetic energy, with more than one-half of the total kinetic energy contributed by horizontal motion of the drops.

The final aspect of this thesis dealt with soil erosion. Specifically,

the timing of water ponding, and soil-water runoff using controlled soil beds for both the rainfall simulator and natural rainfall. The results from the hypothesis that simulated rainfall produces the same soil loss, ponding, and runoff as natural rainfall for events of equal rainfall intensity, remain inconclusive. This is due to the lack of data gathered from the field studies. Many reasons may explain the lack of data, ranging from either the high variability of rainfall rates, near-surface turbulence preventing soil ponding, soil bed designs, and the orientation of soil beds. Simulated rainfall may overestimate the soil loss potential due to the lack of rainfall rate variability and simulation of turbulence. However, there may be an underestimation of soil loss potential from the lack of horizontal wind within the simulator. At this time, no conclusions can be made from this study other than presenting ideas for future research, covered in the following section, to possibly limit the complications this study encountered.

6.2 Future Work

While there were many significant and interesting results taken from this study, there were many valuable aspects that presented themselves during this research and many different directions this research can take. The first, and probably the most important aspect, involves including actual soil loss data that was not possible to collect

during this study, but was attempted. Complications were evident regarding soil bed designs, variability of rainfall rate, and wind in the natural rainfall events. While altering the soil beds to increase the exposure to the rainfall were done, soil loss data was still lacking. More soil beds were made to test a hypothesis that the direction of wind and angle of raindrop impact can affect the exposure of rain to the soil bed. Having soil beds oriented at differing angles relative to each other could minimize the amount of rain that misses the exposed soil in the soil beds. Another idea includes making larger soil exposure beds that could also expose more soil to the natural rainfall.

Another direction this work can take is getting more natural rainfall DSD spectra to analyze. This study was limited to the location of the ACES, whereas having a mobile setup including all the instruments used in this study can increase the number of DSD spectra available for analysis. Other studies discussed in this thesis analyzed large numbers of DSD spectra, whereas only eight were available for analysis in this thesis. Having more data may prove beneficial and more statistically robust.

Another idea for future work is having finer variations in rainfall rate and D_0 using the rainfall simulator. Only the DSDs from two rainfall rates and four different screen heights were analyzed. Since the best potential for the simulated DSDs to replicate natural DSDs

exists with rainfall rates that were similar, having DSD spectra from finer rainfall intensities (varying rainfall rates every 10 mm h^{-1} for example), and altering D_0 with the screen distance at finer resolutions, will provide the best potential for relating natural and simulated rainfall.

The final idea for future work involves simulation of turbulence and horizontal wind. While this aspect is extremely difficult to replicate and represent numerically, a long term goal may involve some type of simulation regarding turbulence. The rainfall simulator used in this study is incapable of replicating turbulence and/or horizontal wind. There may be some simulators in existence that can generate some sort of horizontal wind, but the simulation of turbulence is a direction that could be interesting to pursue regarding natural and simulated rainfall DSDs.

References

Aina, P. O., R. Lal, and G. S. Taylor, 1977: Soil and crop management in relation to soil erosion in the rainforest of western Nigeria. In: G. R. Foster (ed.), Soil erosion: prediction and control. SCSA, Ankeny, Iowa, 75-82.

Atlas, D., and C. W. Ulbrich, 1977: Path-and area-integrated rainfall measurement by microwave attenuation in the 1-3cm band. *J. Appl. Meteor.*, **16**, 1322-1331.

Beard, K., 1985: Simple altitude adjustment to raindrop velocities for Doppler radar analysis. *J. Atmos. & Ocean. Tech.*, **2**, 468-471.

Bisal, F., 1960: The effect of raindrop size and impact velocity on sand splash. *Canad. J. Soil Sci.,* **40**, 242-245.

De Lima, J. L. M. P., P. M. Van Dijk, and W. P. Spaan, 1992: Splash-saltation transport under wind-driven rain. *Soil Tech.*, **5**, 151-166.

Eswaran, H., R. Lal and P.F. Reich. 2001. *Land degradation: an overview.* In: Bridges, E. M., I. D. Hannam, L. R. Oldeman, F. W. T. Pening de Vries, S. J. Scherr, and S. Sompatpanit (eds.). Responses to Land Degradation. Proc. 2nd. International Conference on Land Degradation and Desertification, Khon Kaen, Thailand. Oxford Press, New Delhi, India.

Fox, N. I., 2004: Technical Note: The representation of rainfall drop-size distribution and kinetic energy. *Hydrology and Earth System Sciences*, **8(5)**, 1001-1007.

Helming, K., Ch. H. Roth, R. Wolf und H. Diestel. 1993: Characterization of rainfall-microrelief interactions with runoff using parameters derived from digital elevation models (DEMs). *Soil Tech.,* **6**, 273-286.

_____, 2001: Wind speed effects on rain erosivity. *Sustaining the Global Farm*, 771-776.

Illingworth, A. J., and T. M. Blackman, 2002: The need to represent raindrop size spectra as normalized gamma distributions for the interpretation of polarization radar observations. *J. Appl. Meteorol.*, **41**, 286-297.

_____, 2003: Improved radar rainfall estimates: What index to use in the gamma function for drop spectra? Preprints 31st Conf. on Radar Meteorology. *Amer. Met. Soc.*, Boston, MA, 11-13.

Kinnell, P. I. A., 1983: The effect of kinetic energy of excess rainfall on soil loss from non-vegetated plots. *Aust. J. Soil Res*., **21**, 445-453.

Lack, S. A., and N. I. Fox, 2003: Correcting radar derived rainfall rates at the surface using Doppler velocities. Preprints 31st Conf. on Radar Meteorology. *Amer. Met. Soc.*, Boston, MA.

Laws, J. O. and Parsons, D. A., 1943: The relation of raindrop size to intensity. *Trans. Amer. Geophys. Un.*, **24**, 452-460.

Marshall, J. S. and W. McK. Palmer, 1948: The distribution of raindrops with size. *J. Meteorol*., **5**, 165-166.

Mason, B. J. and J. B. Andrews, 1960: Drop size distribution from various types of Rain. *Quart. J. Roy. Met. Soc*., **86**, 346-353

Meyer, L. D., 1965: Simulation of rainfall for soil erosion research. *Trans. ASAE*, **8**, 63-65.

Mutchler, C. K. and L. F. Hermsmeier, 1965: A review of rainfall simulators. *Trans. ASAE*, **8,** 67-68.

Parsons, D. A., 1943: Discussion of the application and measurement of artificial rainfall on types FA and F infiltrometer. *Amer. Geophys. Union Trans.,* **24**, 485-487.

Pedersen, H. S. and B. Hasholt, 1995: Influence of wind speed on rainsplash erosion. *Catena*, **24**, 39-54.

Regmi, T. P. and A. L. Thompson, 2000: Rainfall simulator for laboratory studies, *Amer. Soc. Ag. Eng.*, **16(6)**, 641-647.

Renard, K. G., G. R. Foster, G. A. Weesies, D. K. McCool, and D. C. Yoder, 1997: Predicting soil erosion by water: A guide to conservation planning with the Revised Universal Soil Loss Equation (RUSLE). *U.S. Department of Agriculture, Agriculture Handbook No. 703.*

Schwab, G. O., D. D. Fangmeier, W. J. Elliot, and R. K. Frevert, 1993: *Soil and Water Conservation Engineering*. John Wiley and Sons, Inc., 507 pp.

Stillmunkes, R. T. and L. G. James, 1982: Impact energy of water droplets from irrigation sprinklers. *Trans. ASAE,* **25**, 130-133.

Testud, J., S. Oury, R. A. Black, P. Amayenc, and D. Xiankang, 2001: The concept of "normalized" distribution to describe raindrop spectra: a tool for cloud physics and cloud remote sensing. *J. Appl. Meteorol*., **40**, 1118-1140.

Thompson, A. L. and L. G. James, 1985: Water droplet impact and its effect on infiltration. *Trans. ASAE,* **28**, 1506-1520.

_____, and F. Ghidey. 2000: Soil in Motion. *ASAE Resource magazine*, 8 December 2000 issue, 7 pp.

Ulbrich, C. W., 1983: Natural variations in the analytical form of the raindrop size distribution. *J. Clim. Appl. Meteorol.*, **22**, 1764-1775.

_____, and D. Atlas, 1998: Rainfall microphysics and radar properties: Analysis methods for drop size spectra. *J. Appl. Meteorol.*, **37**, 912-932.

Van Dijk, A. I. J. M., L. A. Bruijnzeel, and C. J. Rosewell, 2002: Rainfall intensity – kinetic energy relationships: a critical literature appraisal. *J. Hydrol.,* **261,** 1-23.

Wishmeier, W. H. and D. D. Smith., 1958: Rainfall energy and its relationship to soil loss. *Trans. Amer. Geophys. Un.,* **39**, 285-291.